PRESENCE OF CARBON-BASED NANOSTRUCTURES IN ELECTRON-BEAM IRRADIATED FOOD PRODUCTS

A Thesis

Presented to

The Faculty of the Department of Engineering Technology

University of Houston

In Partial Fulfillment

Of the Requirements for the Degree of

Master of Science in

Engineering Technology

By

Jennifer T. Nguyen

May 2015

PRESENCE OF CARBON-BASED NANOSTRUCTURES IN ELECTRON-BEAM IRRADIATED FOOD PRODUCTS

_____

Jennifer T. Nguyen

APPROVED:

_____

Dr. Francisco C. Robles Hernández

_____

Dr. Rupa Iyer

_____

Dr. T. Randall Lee

_____

Dr. Jack A. Neal

_____

Dr. Rupa Iyer
Associate Dean of Research and Graduate Studies of the College of Technology

_____

Dr. Wajiha Shireen
Chair of Engineering Technology

ACKNOWLEDGMENTS

During my time at the University of Houston, I have been very fortunate to come across many people with whom I have shared my experiences.

I would like to thank my three advisors for their insight, comments, and feedback throughout the duration of this project. I am grateful to Dr. Francisco C. Robles Hernández for reminding me to always continue forward, Dr. Jack A. Neal for encouraging me to look even farther ahead, and Dr. T. Randall Lee for your continual support from before I had even entered into the graduate program.

I appreciate the overwhelming support from Anderson Okonkwo and the Lee Research Group: Amin, Arati, Chris, Chulsoon, Crystal, Dahye, Daniela, Ging, Han Ju, Henry, Jack, Jeck, Johnson, Long, Maria, Oussama, Tingting, and Yi-Ting. Also, this appreciation is extended to the Miljanić Research Group, who unofficially adopted me into their group: Chia-Wei, Ha, Ljuba, Mohamed, Musabbir, Nadia, Rio, Qing, Xiao, and another unofficial member Alan.

I wish to thank my family for their unwavering support and unconditional faith throughout this journey in academic and professional growth. I would like to make a special mention to An Nguyen, who always had the best response and continually reminded me of my purpose in enduring these past few years.

Finally, I want to thank Dr. Rupa Iyer for your prompt and gracious response, despite having been given a short amount of time with my work.

PRESENCE OF CARBON-BASED NANOSTRUCTURES IN ELECTRON-BEAM IRRADIATED FOOD PRODUCTS

An Abstract of a Thesis

Presented to

The Faculty of the Department of Engineering Technology

University of Houston

In Partial Fulfillment

Of the Requirements for the Degree of

Master of Science in

Engineering Technology

By

Jennifer T. Nguyen

May 2015

ABSTRACT

Previous studies have shown electron-beam (e-beam) irradiation to be effective in eliminating mold in natural products. More recently, we found the presence of rod-like nanostructures in natural and composite corks following e-beam irradiation. Here, we present an investigation on the effects of e-beam irradiation on wine corks and selected herbs. Chapter 1 reviews the safety of irradiation on food, while briefly covering the health safety of carbon-based nanostructures. Chapter 2 reports the characterization of the nanostructures, herein referred to as nanorods (NRs), found in the commercially irradiated corks, after having been irradiated with 5, 10, and 15 kiloGrays (kGy) from an e-beam. We found larger radiation doses were not necessarily more effective in producing NRs. The characterization of the NRs was carried out by means of energy-dispersive x-ray spectroscopy (EDX), Raman spectroscopy, scanning electron microscopy (SEM), and transmission electron microscopy (TEM). Characterization showed dissimilarities between the NRs isolated from irradiated corks and known characteristics of carbon nanotubes (CNTs) used for reference; however, the presence of oxygen (O) in the NR structure suggests a different nanostructure possibly not previously identified. Chapter 3 demonstrates similar nanostructure formation from e-beam irradiation on the selected herbs and spices: basil, cilantro, oregano, parsley, and flour. The herbs and spices were irradiated with 1, 3, and 5 kGy. Similar to the case of e-beam irradiation of corks, larger radiation doses did not necessarily produce more nanostructures. Finally in Chapter 4, conclusions, perspectives, and future work based on Chapter 2 and 3 are presented.

TABLE OF CONTENTS

LIST OF FIGURES

LIST OF TABLES

Chapter I. Introduction to Irradiation and Carbon-Based Nanomaterials

1.1. Introduction: Why Irradiate?

Irradiation is a safety measure adopted by both the food and non-food industries to treat and/or eliminate microorganisms. According to the U.S. Center for Disease Control, foodborn diseases are responsible for millions of occurrences of illness, thousands of deaths, and millions of dollars spent on treatment.[1] The implications regarding the necessity to irradiate food are global.[2] Ionizing irradiation, initially introduced as a method to improve the quality and shelf life of foods, is used by the food industry as a safety measure to eliminate bacteria, molds, and related species, particularly with imported food products, such as spices and flour.[3-7]

The United States is a heavy importer and consumer of herbs and spices.[8] However, consumers are unaware of the heavy microbial load herbs and spices carry, especially imported ones.[9] Most imported herbs and spices already undergo ionizing irradiation, and can be identified by the Radura symbol on the packaging. Additionally, multi-ingredient foods can also include irradiated ingredients but do not need to be labeled, such as dried oregano in tomato sauce.[2] Irradiation is the preferred method for decontamination in herbs and spices because it is a cold process, and unlike other decontamination methods, such as steam or fumigation by ethylene oxide, it does not affect the aroma and flavor of the irradiated products.[10] This technology developed for conducting food irradiation has long been used for the sterilization of medical devices and cosmetic products, and is currently being evaluated on wine corks.[11]

Irradiation of wine corks can prove effective in eliminating the mold responsible for wine taint. Various molds present in wine corks react with 2,4,6-trichlorophenol (TCP) via O-methylation to produce 2,4,6-trichloroanisole (TCA), a common culprit causing wine taint, as

represented in **Figure 1.1**. At low concentrations in as small an amount as 1.4 ppt, TCA is capable of distorting scents by suppressing olfactory signal transduction, and is perceived by unfavorable odors, such as that of a moldy newspaper or wet dog.[12] Wine taint, in addition to contaminating that particular bottle of wine, can contribute to discontinued patronage of a winery or restaurant, accounting for an estimated $10 billion loss annually.[13] To eliminate the source of wine taint, wine producers have tried moving toward alternative wine stoppers, such as those made from plastic or aluminum. However, plastic stoppers allow for too much oxygen to enter the wine, while aluminum allows for too little oxygen to enter, and thus adversely affects the wine quality by improper aging.[14] Also, both aluminum and plastic wine stoppers involve nonrenewable synthetic plastic, while cork is a renewable resource that can be regenerated from tree bark many times, on average about 15 times in the tree's lifetime.[15]

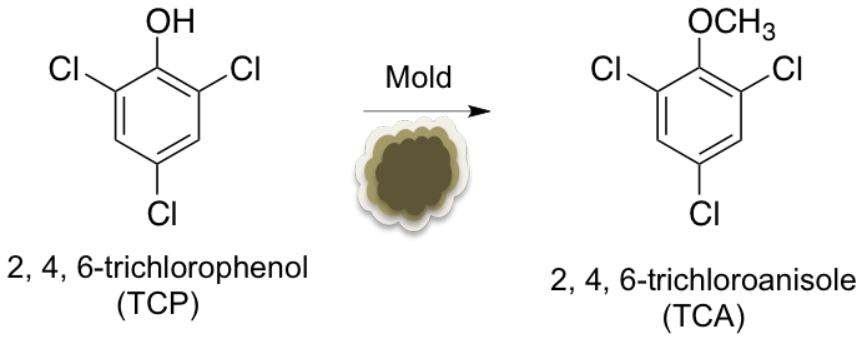

Figure 1.1. Representation of the conversion of TCP to TCA in the presence of mold

Early investigations by the U.S. Army found that food exposed with a dose of irradiation up to 10 kGy proved safe for consumption; a conclusion based upon the observation that irradiation posed no toxicological hazards, or special nutritional or microbiological concerns.[3] A joint study group of the Food Agriculture Organization of the United Nations, International

Atomic Energy Agency, and World Health Organization concluded that exposing foods to ionizing radiation was similar to processing them with thermal treatments, similar to those used in canning procedures to reduce pathogens and spoilage, and that the procedure maintained the food's non-hazardous integrity.[3] With herbs and spices, most countries already approve doses up to 10 kGy, and the United States allows up to 30 kGy.[10] However, any information on the effect of irradiation on food packaging products such as cork is sorely lacking.

1.2. Irradiation: Types, Mechanisms, and Sources

Currently, irradiation of food products is carried out using either ionizing or non-ionizing radiation. Energy absorbed by food from ionizing radiation, the absorbed dose, leads to the excitation of atoms and molecules in food, which in turn might cause electrons to be ejected from the molecule, leaving behind positively charged cations.[3] This process produces unpaired electrons, essentially highly reactive free radicals, which may ionize other molecules, as represented in **Figure 1.2**. The primary ion formations occur in the first 10^{-14} s of radiation exposure, while secondary processes, such as subsequent ionization coming from the initial ions, occur over a 10^{-2} s timeframe.[3] Neutralization might occur through the combination of radicals, while displaced electrons might be physically trapped or recombine with positive ions. In terms of inactivating microorganisms, sufficient irradiation can destroy their reproductive ability.[16] All components of the microorganism are susceptible to the effects of exposure to radiation, with nucleic acids found to be the most sensitive to these treatments. The depolymerization of DNA occurs from intensive exposure to ionizing irradiation, where lesions in both strands of polynucleotides exceed enzymatic repair processes, disabling DNA function. Also, disruption of the base pairs in DNA can lead to crosslinking of the strands, preventing unraveling during

mitosis. In general, microorganisms can be arranged in order of increasing resistance to radiation: vegetative bacteria, fungi and fungal spores, bacterial spores, viruses, and prions.[16]

In contrast, non-ionizing irradiation, such as UV irradiation, while effective for disinfecting water, has no capacity to break molecular bonds consistently.[17] Instead, non-ionizing radiation provides enough energy for excitation of molecules, which in turn can produce a temperature change, and sometimes ionization and bond breakage, as seen in **Figure 1.2**. UV irradiation is capable of targeting nucleic acids inside cells while maintaining cellular integrity.[18] However, a recent study showed that *Escherichia coli* and *Pseudomonas aeruginosa* in water could be induced into a type of dormant state, a viable but non-cultureable (VBNC) state, from UV irradiation, and that they might be resuscitated given optimum conditions of temperature and nutrients.[18] The idea of incomplete microorganism-deactivation makes non-ionizing radiation less favorable, as compared to ionizing radiation treatments, for eliminating microorganisms on food products.

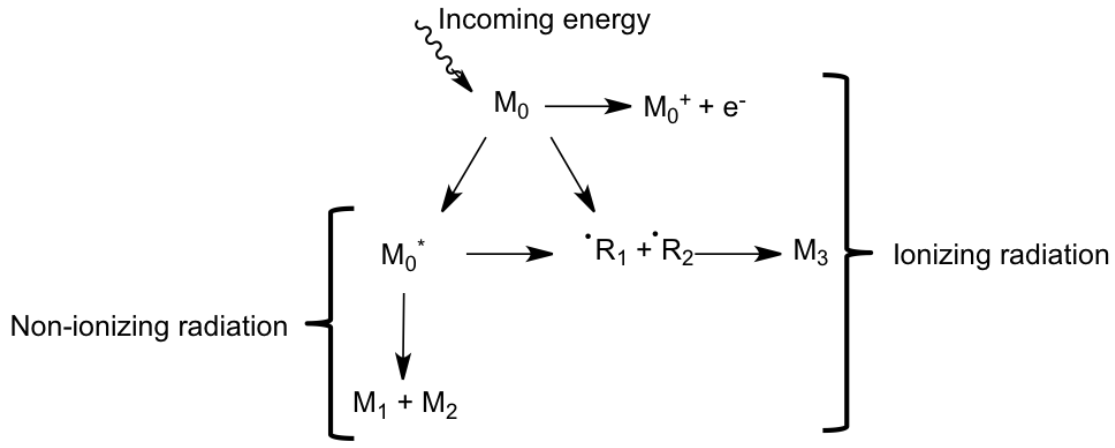

Figure 1.2. General molecular products from non-ionizing and ionizing radiation treatments, where M indicates molecules and R radical molecules.

The three sources of approved ionizing radiation are γ-rays, x-rays, and electron beams (e-beams).[2] The radioisotope of Cobalt-60 (Co-60) is the source of γ-rays; however the Co-60

source has to be stored in water to absorb its emitted radiation when not in use. This special storage requirement, in addition to the limited worldwide supply of Co-60, makes γ-rays a less attractive method for irradiation.[3] Another option for an irradiation source is the use of a high voltage e-beam accelerated by linear accelerators to high speeds in a vacuum tube, controlled easily by a switch. The e-beams do not need the special storage or replenishment of the source associated with Co-60, but they have a shallower depth of penetration. E-beams can either be directly targeted on the sample to be irradiated, giving rise to a higher energy dose than that obtained with x-rays, and shorter exposure and processing times, or be targeted toward heavy metals that give off bremsstrahlung x-rays, which are more penetrating than γ-rays and e-beam electrons, as represented in **Figure 1.3**. However, the resulting bremsstrahlung x-rays possess a lower energy than the initial electron energy that generated these x-rays. X-ray irradiation thus requires a longer processing time to accumulate the appropriate dosage as compared to direct e-beam irradiation.[3]

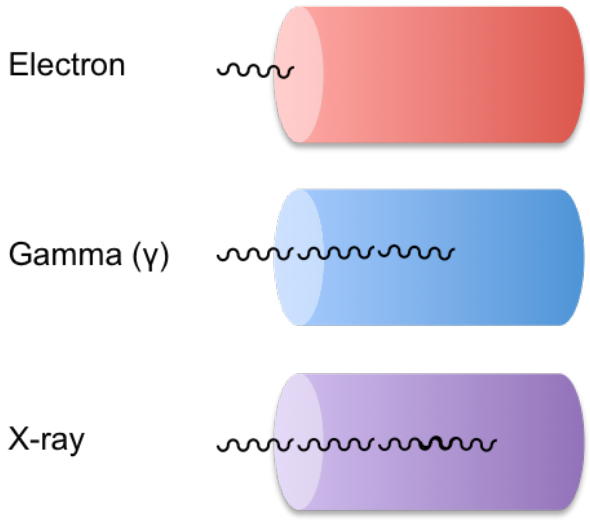

Figure 1.3. Representation of the penetration depth from each source of radiation. Penetration depth is dependent on the energy of the incoming radiation and density of target material, usually a few centimeters for e-beam irradiation and several meters for γ- and x-rays.[16]

It is important to note that while irradiation from Co-60 generates enough energy to penetrate and ionize atoms and molecules within a target, Co-60 lacks sufficient energy to create other radioisotopes. Radiation from Co-60 cannot render other materials, like the target foods, radioactive.[16]

A previous study has demonstrated that commercial e-beam irradiation is effective in reducing or eliminating mold in wine cork stoppers below the detectable limit of 0.8 CFU/g with doses as low as 5 kGy.[11] The presence of mold has been quantified by microbial enumeration of pulverized cork samples in both pre- and post-irradiation treatments. While this irradiation treatment showed a significant reduction in microbial colony formations, small protruding fibers resembling carbon nanotubes were subsequently observed on these corks. Similar effects have not been observed on other irradiated foods or non-food products.[19, 20]

Herbs and spices have also undergone extensive studies from ionizing irradiation treatments. Soriani *et al.* concluded γ-irradiation of ginkgo and guarana was effective in reducing microbial contamination while maintaining the flavor integrity of ginkgo and the caffeine content of guarana based on microbial colony counts and high-performance liquid chromatography (HPLC), respectively.[21] Minea *et al.* came to similar conclusions from e-beam irradiation on fresh herbs, sage, and marigold, based on microbial colony counts and antioxidant activity from lipid peroxidation measurements.[22] Few other previous studies on irradiation of herbs and spices examined for any visual changes by high magnification microscopy such as scanning electron microscopy (SEM) or transmission electron microscopy (TEM). Work by Lee et al. on γ-irradiated corn starch found no changes in corn starch granules,[20] while Kwon *et al.* observed a significant increase in the surface roughness of 10 kGy γ-irradiated starch from corn.[19]

1.3. Toxicity of Carbon Nanotubes

Nanoparticles continue to be studied due to their potential and in some cases clinical biomedical applications,[23, 24] including drug delivery.[25-27] Nanotubes have gained attention for targeted drug delivery because of their distinct inner and outer surfaces, removable end caps, and increased volume over other nanoparticle systems that allows for a higher payload capacity.[28] Carbon nanotubes (CNTs) can exist as single-walled carbon nanotubes (SWCNTs) or multi-walled carbon nanotubes (MWCNTs). Conclusions from pulmonary toxicity studies of CNTs are inconsistent, with outcomes showing either no effects, both short and long term effects, or negative effects, namely, cell apoptosis, necrosis, DNA damage, and cell death.[29] Studies showing no changes include guinea pigs treated with CNTs from arc sublimation of graphite[30] and mice given a treatment of 0.5 mg of nickel-containing CNTs.[31] However, the same study of the nickel-containing CNTs also showed evidence of congestion and postmortem histopathological changes in the lungs of the mice dying from CNT exposure; the surviving mice had large aggregates of particles in macrophages in the alveolar space, some of which were found in the interstitium as granulomas. A different study of mice using the same CNT dosage found 15% mortality due to mechanical blockage of the upper airways, while the surviving mice appeared normal throughout the duration of the study.[32]

Given the similarities in physical shape and possible bodily effects to asbestos, MWCNTs are believed to pose a threat by their potential to cause inflammation and mesothelioma, as represented in **Figure 1.4**.[29] Maladies arising from CNTs may be due to their inert, rigid, high-aspect ratio structure; essentially, they are rigid rods that are difficult to break down, with longer MWCNTs causing more potent problems.[29] *Ex situ* experiments involving liver and mesothelial cells showed MWCNTs entering the cell via tip entry, where the nanotube

is perpendicular to the cell surface. MWCNTs lying flat on the membrane showed no visible signs of cellular uptake. However, the membrane receptors cluster around the end caps of the more perpendicular MWCNTs and initiate uptake of what the receptors think is a small, rounded particle. This action is followed by a relatively rapid strain-induced transition to near-vertical fiber alignment, providing no opportunity for the membrane to sense the ultimate length of the MWCNT. Eventually, the endosomes are unable to internalize and package the MWCNT, thus leading to incomplete endocytosis, which can lead to chronic inflammation, granuloma development, and cell death by apoptosis.[33] The incomplete internalization is more pronounced in CNTs with longer lengths since longer fibers are unlikely to navigate past the diaphragm or pleural cavity; therefore, those with shorter lengths caused no significant inflammation.[33] In liver cells, incomplete endocytosis leads failure of internalization into lysosomes, followed by physical interference with cytoskeletal-mediated processes, including protein and lipid secretion, and biliary transport.[34] Another factor that determines toxicity is the diameter of the CNT—thinner MWCNTs being more toxic than thicker ones. *In vitro* and *in vivo* experiments of 5 μm long MWCNTs showed that those with a thinner diameter (9.4 nm) were toxic toward alveolar macrophages and induced inflammatory lung response in rats, while those with a thicker diameter (70 nm) presented little toxicity.[35]

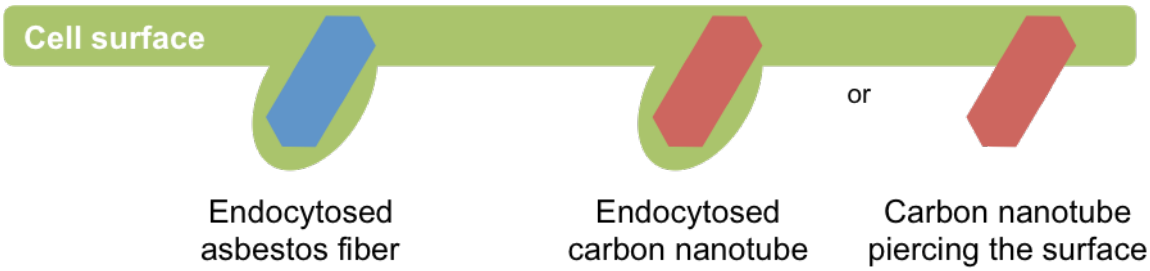

Figure 1.4. Physical similarity of asbestos fibers to CNTs is also seen in their respective methods of cell entry, where asbestos is endocytosed while CNTs can enter through endocytosis or piercing of the cell.[36]

The surface properties of CNTs also affect toxicity. Pristine CNTs are chemically inert and incompatible with nearly all solvents; upon functionalization by oxidation for improving uptake, CNTs are more capable of damaging the body due to their incompatibility with body tissue.[33, 37] A study showed acid-based polymer-coated MWCNTs were readily introduced into macrophages, where they induced inflammation, while polystyrene-based polymer-boated MWCNTs did not enter macrophages as easily.[38] SWCNTs also showed similar results, where acid-functionalized SWCNTs were more potent due to increased dispersibility and surface charge. The acid-functionalized SWCNTs induced mouse lung epithelial cell cycle arrest and lung inflammation more than than pristine SWCNTs, where they also enhanced cardiac toxicity after pulmonary exposure.[39] With the introduction of defects in the CNT structure, the oxidized functionalities are partially reduced, so there is a lessened level of toxicity in functionalized CNTs with defects as compared to those without defects.[40]

Bio-durability, that is, the durability of the CNT once inside the organism, is also an important factor in determining the toxicity of the CNT.[33] CNTs have survived 2 years after introduction to the cell both at the site of exposure, and elsewhere in the body.[41] Similarly, CNT clusters surrounded by macrophages were also detectable 2 years after an initial exposure.[42] A study comparing SWCNTs, with and without defects incubated in hydrogen peroxide, noted that

the defective SWCNT decreased in length by 45% at 8 weeks and further decreased in diameter over time.[43] The pristine SWCNT showed no degradation, indicating that defects or functionalization possibly act as sites for the interactions responsible for the CNT degradation. However, the underlying degradation mechanism is currently unknown, and there remains the question as to how harmful the by-products from CNT degradation might be, in addition to the harmful effects of the CNTs themselves.

1.4. Research Objectives

Cork sterilization by radiation started with γ irradiation on corks containing mold, TCP, and TCA, leading to the elimination of mold, but not the inactivation of the TCA already present in the cork.[44] Other studies have focused on the effects of e-beam treatment on the TCA already present in cork. Doses of 25-50 kGy degraded TCA to mono and dichloroanisoles,[45] while doses above 100 kGy eliminated TCA;[46] however, doses above 100 kGy are not currently approved on any commercially available product. Alternatively, e-beam irradiation of wine corks to eliminate mold before it converts TCP to TCA is a fairly new idea under investigation, and not yet put into practice.[11] The irradiation of the corks used to seal wine bottles successfully eliminates the mold that is responsible for active formation of TCA, theoretically providing taint-free corks.

This study provides evidence of the formation of nanostructures after irradiation treatment. The presence of such nanostructures, resembling nanotubes in commercially irradiated wine corks, poses a potential health risk to workers handling the corks, as well as consumers of the products using the irradiated cork packaging. My research has focused on identifying the nanostructures found in commercially irradiated wine corks, "as purchased" and after inoculation with mold, using various instrumental techniques: SEM, TEM, and

spectroscopic analysis, energy-dispersive x-ray spectroscopy (EDX), and Raman spectroscopy. The resulting data obtained from this work were compared to the known properties of CNTs.

Furthermore, dried herbs (e.g., basil, cilantro, oregano, and parsley) and flour were commercially irradiated and examined for similar nanostructure formation as that found in the wine bottle corks exposed to e-beam irradiation by microscopy. Previous investigations on the effects of irradiation on herbs and spices have been limited to microbiological safety, safety of chemical changes, and nutritional adequacy. Results from this work would be the first microscopy efforts of the chosen herbs and flour from e-beam irradiation.

The following are the objectives of the present work: the characterization of nanostructure formation in corks and other natural products subjected to e-beam irradiation; to correlate statistically the presence of the nanostructures with absorbed radiation dosage; and to investigate the chemical composition of the nanostructures by means of EDX and Raman spectroscopy.

1.5. Research Outline

This thesis is organized into four chapters. The present chapter presents a brief introduction to the sterilization of food and food packaging products by irradiation as well as an introduction to the toxicity of carbon-based nanomaterials. Chapter 2 describes the preparation of irradiated wine corks and characterization of the nanostructures found therein by microscopy and spectroscopy. Chapter 3 describes the analysis of similarly prepared irradiated dried herbs (e.g., basil, cilantro, oregano, and parsley) and flour, also characterized by microscopy. Finally, Chapter 4 summarizes key points of the projects from Chapters 2 and 3 with an overall conclusion of the thesis, including proposed future research work.

1.6. References

(1) Centers for Disease Control and Prevention, National Center for Emerging and Zoonotic Infectious Diseases, Division of Foodborne, Waterborne, and Environmental Diseases. CDC Estimates of Foodborne Illness in the United States. *Fact Sheet Findings-CDC 2011 Estimates*.

(2) The U.S. Food and Drug Administration Center for Food Safety and Applied Nutrition Food Information. Food Irradiation: What You Need to Know. *2014 Fact Sheet-Food Facts from the U.S. Food and Drug Administration*.

(3) Molins, R.A., *Food Irradiation: Principles and Applications*. John Wiley & Sons: Chichester, UK, **2001**.

(4) Neal, J.A.; Cabrera-Diaz, E.; Marquez-Gonzalez, M.; Maxim, J.E.; Castillo, A. Reduction of Escherichia coli O157:H7 and Salmonella on baby spinach, using electron beam radiation. *J Food Prot* **2008**, *71*, 2415-2420.

(5) Blank, G.; Shamsuzzaman, K.; Sohal, S. Use of electron beam irradiation for mold decontamination on cheddar cheese. *J Dairy Sci* **1992**, *75*, 13-18.

(6) Chelack, W.S.; Borsa, J.; Marquardt, R.R.; Frohlich, A.A. Role of the competitive microbial flora in the radiation-induced enhancement of ochratoxin production by Aspergillus alutaceus var. alutaceus NRRL 3174. *Appl. Environ. Microbiol.* **1991**, *57*, 2492-2496.

(7) Koorapati, A.; Foley, D.; Pilling, R.; Prakash, A. Electron-beam irradiation preserves the quality of white button mushroom (Agaricus bisporus) slices. *J. Food Sci.* **2003**, *69*, SNQ25-SNQ29.

(8) Buzzanell, P.J.; Dull, R.; Gray, F. The Spice Market in the United States: Recent Developments and Prospects. *Agriculture Information Bulletin No. 709*, **1995**.

(9) Lochhead, C. The High-tech Food Process Foes Find Hard to Swallow. *Food Tech.* **1989**, *43*, 56-60.

(10) Peter, K.V., *Handbook of herbs and spices, Vol. 3*. CRC Press: Boca Raton, FL, **2006**.

(11) Corsi, A.J. The Effectiveness of Electron Beam Irradiation to Significantly Reduce or Eliminate Molds Known to Cause 2,4,6-Trichloroanisole in Cork Stoppers. M.S. Thesis, University of Houston, Houston, TX, 2011.

(12) Takeuchi, H.; Kato, H.; Kurahashi, T. 2,4,6-Trichloroanisole is a potent suppressor of olfactory signal transduction. *Proc. Natl. Acad. Sci. U.S.A.* **2013**, *110*, 16235-16240.

(13) Fuller, P. Cork taint—closing in on an industry problem. *Aust. N. Z. Wine Ind. J.* **1995**, *10*, 58-60.

(14) Lopes, P.; Saucier, C.; Glories, Y. Nondestructive Colorimetric Method To Determine the Oxygen Diffusion Rate through Closures Used in Winemaking. *J. Agric. Food Chem.* **2005**, *53*, 6967-6973.

(15) Dharmadhilari, M. Wine Corks. *Vineyard & Vintage View* **1994**, *9*, 1-8.

(16) Fairand, B.P., *Radiation Sterilization for Health Care Products: X-Ray, Gamma, and Electron Beam*. CRC Press: Boca Raton, FL, **2001**.

(17) Cao, C.; Sim, S.J. Signal enhancement of surface plasmon resonance immunoassay using enzyme precipitation-functionalized gold nanoparticles: A femto molar level measurement of anti-glutamic acid decarboxylase antibody. *Biosens. Bioelectron.* **2007**, *22*, 1874-1880.

(18) Zhang, S.; Ye, C.; Lin, H.; Lv, L.; Yu, X. UV Disinfection Induces a Vbnc State in Escherichia coli and Pseudomonas aeruginosa. *Environ. Sci. Technol.* **2015**, *49*, 1721-1728.

(19) Kwon, J.-H.; Kim, S.-J.; Lee, J.; Lee, S.-J.; Kim, S.-K.; Kim, J.-S.; Byun, M.-W. Physicochemical and Organoleptic Properties of Starch Isolated from Gamma-Irradiated Acorn. *Korean J. Food Sci. Technol.* **2002**, *34*, 1007-1012.

(20) Lee, Y.-J.; Kim. S.Y.; Lim, S.-T.; Han, S.-M.; K. H.-M.; Kang, I.-J. Physicochemical Properties of Gamma-Irradiated Corn Starch. *J. Food. Sci. Nutr.* **2006**, *11*, 146-154.

(21) Soriani, R.R.; Satomi, L.C.; Pinto, T.J.A. Effects of ionizing radiation in ginkgo and guarana. *Radiat. Phys. Chem.* **2005**, *73*, 239-242.

(22) Minea, R.; Nemtanu, M.R.; Brasoveanu, M. Oproiu, C. Accelerators use for irradiation of fresh medicinal herbs. *Proceedings of EPAC* **2004**, 2371-2373.

(23) Colombo, M.; Carregal-Romero, S.; Casula, M.F.; Gutierez, L.; Morales, M.P.; Bohm, I.B.; Heverhagen, J.T.; D., P.; Parak, W.J. Biological applications of magnetic nanoparticles. *Chem. Soc. Rev.* **2012**, *41*, 4306-4334.

(24) Singamaneni, S.; Bliznyuk, V.N.; Binek, C.; Tsymbal, E.Y. Magnetic nanoparticles: recent advances in synthesis, self-assembly and applications. *J. Mater. Chem.* **2011**, *21*, 16819-16845.

(25) Arruebo, M.; Fernandez-Pacheco, R.; Ibarra, M.; Santamaria, J. Magnetic nanoparticles for drug delivery. *Nanotoday* **2007**, *2*, 22-32.

(26) Kami, D.; Takeda, S.; Itakura, Y.; Gojo, S.; Watanabe, M.; Toyoda, M. Application of magnetic nanoparticles to gene delivery. *Int. J. Mol. Sci.* **2011**, *12*, 3705-3722.

(27) Dobson, J. Magnetic nanoparticles for drug delivery. *Drug Dev. Res.* **2006**, *67*, 55-60.

(28) Hilder, T.A.; Hill, J.M. Carbon nanotubes as drug delivery nanocapsules. *Current Applied Physics* **2008**, *8*, 258-261.

(29) Nerl, H.C.; Cheng, C.; Goode, A.E.; Bergin, S.D.; Lich, B.; Gass, M.; Porter, A.E. Imaging methods for determining uptake and toxicity of carbon nanotubes in vitro and in vivo. *Nanomedicine (London, U. K.)* **2011**, *6*, 849-865.

(30) Huczko, A.; Lange, H.; Calko, E.; Grubek-Jaworska, H.; Droszcz, P. Physiological testing of carbon nanotubes: are they asbestos-like? *Fullerene Sci. Technol.* **2001**, *9*, 251-254.

(31) Lam, C.-W.; James, J.T.; McCluskey, R.; Hunter, R.L. Pulmonary Toxicity of Single-Wall Carbon Nanotubes in Mice 7 and 90 Days After Intratracheal Instillation. *Toxicol. Sci.* **2004**, *77*, 126-134.

(32) Warheit, D.B.; Laurence, B.R.; Reed, K.L.; Roach, D.H.; Reynolds, G.A.M.; Webb, T.R. Comparative Pulmonary Toxicity Assessment of Single-wall Carbon Nanotubes in Rats. *Toxicol. Sci.* **2004**, *77*, 117-125.

(33) Lanone, S.; Andujar, P.; Kermanizadeh, A.; Boczkowski, J. Determinants of carbon nanotube toxicity. *Adv. Drug Delivery Rev.* **2013**, *65*, 2063-2069.

(34) Shi, X.; von dem Bussche, A.; Hurt, R.H.; Kane, A.B.; Gao, H. Cell entry of one-dimensional nanomaterials occurs by tip recognition and rotation. *Nat. Nanotechnol.* **2011**, *6*, 714-719.

(35) Fenoglio, I.; Aldieri, E.; Gazzano, E.; Cesano, F.; Colonna, M.; Scarano, D.; Mazzucco, G.; Attanasio, A.; Yakoub, Y.; Lison, D.; Fubini, B. Thickness of Multiwalled Carbon Nanotubes Affects Their Lung Toxicity. *Chem. Res. Toxicol.* **2012**, *25*, 74-82.

(36) Nagai, H.; Toyokuni, S. Differences and similarities between carbon nanotubes and asbestos fibers during mesothelial carcinogenesis: Shedding light on fiber entry mechanism. *Cancer Sci.* **2012**, *103*, 1378-1390.

(37) Magrez, A.; Kasas, S.; Salicio, V.; Pasquier, N.; Seo, J. W.; Celio, M.; Catsicas, S.; Schwaller, B.; Forró, L. Cellular Toxicity of Carbon-Based Nanomaterials. *Nano Lett.* **2006**, *6*, 1121-1125.

(38) Tabet, L.; Bussy, C.; Setyan, A.; Simon-Deckers, A.; Rossi, M.; Boczkowski, J.; Lanone, S. Coating carbon nanotubes with a polystyrene-based polymer protects against pulmonary toxicity. *Part. Fibre Toxicol.* **2011**, *8*, 3-15.

(39) Saxena, R.; Williams, W.; McGee, J.; Daniels, M.; Boykin, E.; Gilmour, I. Enhanced *in vitro* and *in vivo* toxicity of poly-dispersed acid-functionalized single-wall carbon nanotubes. *Nanotoxicology* **2007**, *1*, 291-300.

(40) Muller, J.; Huaux, F.; Fonseca, A.; Nagy, J. B.; Moreau, N.; Delos, M.; Raymundo-Piñero, E.; Béguin, F.; Kirsch-Volders, M.; Fenoglio, I.; Fubini, B.; Lison, D. Structural Defects Play a Major Role in the Acute Lung Toxicity of Multiwall Carbon Nanotubes: Toxicological Aspects. *Chem. Res. Toxicol.* **2008**, *21*, 1698-1705.

(41) Deng, X.; Jia, G.; Wang, H.; Sun, H.; Wang, X.; Yang, S.; Wang, T.; Liu, Y. Translocation and fate of multi-walled carbon nanotubes in vivo. *Carbon* **2007**, *45*, 1419-1424.

(42) Muller, J.; Delos, M.; Panin, N.; Rabolli, V.; Huaux, F.; Lison, D. Absence of Carcinogenic Response to Multiwall Carbon Nanotubes in a 2-Year Bioassay in the Peritoneal Cavity of the Rat. *Toxicol. Sci.* **2009**, *110*, 442-448.

(43) Allen, B.L.; Kichambare, P.D.; Vlasova, I.I.; Kapralov, A.A.; Konduru, N.; Kagan, V.E.; Star, A. Biodegradation of single-walled carbon nanotubes through enzymatic catalysis. *Nano Lett.* **2008**, *8*, 3899-3903.

(44) Pereira, C.; Gil, L. Radiation in Cork Treatments. In *Radiation Physics Research Progress*; Camilleri, A.N., ed.; Nova Science: New York, NY, 2008.

(45) Careri, M.; Mazzoleni, V.; Musci, M.; Molteni, R. Study of Electron Beam Irradiation Effects on 2,4,6-Trichloroanisole as a Contaminant of Cork by Gas Chromatography-Mass Spectroscopy. *Chromatographia* **2001**, *53*, 553-557.

(46) Mazzoleni, V.; Molteni, R.; Furni, M.D.; Musci, M. Effect of accelerated electron beam irradiation on cork used for stopper production. *Ind. Bevande* **2000**, *29*, 247-257.

Chapter II. Characterization of Nanostructures Observed in Cork

2.1. Introduction

Electron-beam (e-beam) irradiation of foods has been utilized in the food industry for many years to prevent the spread of contamination from bacteria, molds, and related species.[1] In the case of treating wine corks, e-beam irradiation is a newly-introduced idea to eliminate the mold responsible for wine taint.[1] The mold in the wine cork reacts with 2,4,6-trichlorophenol (TCP), a chemical commonly found in corks,[2] to produce 2,4,6-trichloroanisole (TCA), which can be readily transferred to the wine. TCA is detectable to the human palate at levels as low as 1.4 ppt and has an unpleasant odor described as a moldy newspaper, wet dog, or damp cloth, which can overpower any flavors present in the wine. By eliminating mold, and thus TCA formation, billions of dollars can be saved annually from lost revenue from spoiled or tainted wine. A number of efforts have been made to accomplish this task, including the use of ionizing radiation. However, a previous study observed the formation of carbon nanotube-like structures that appeared to be associated with the mold decontamination procedure.[3] The presence of such nanostructures in commercially irradiated wine corks, poses a potential health risk to workers handling the corks, as well as to consumers of the products using the irradiated cork packaging.[4,5] Corsi *et al*. are currently investigating the decontamination efficiency of e-beam irradiation on wine corks through the determination of the "D-value". The D-value is defined as the decimal reduction time; in this case, the radiation dosage required to reduce the number of viable organisms by one logarithmic unit, or 90%.[6]

This chapter reports the analysis and characterization of nanostructures found in wine corks, particulate materials first reported by Corsi *et al*.[3] The nanostructures were shaped like

rods and these nanorods (NRs) were observed in both non-irradiated and irradiated wine corks at various absorbed radiation dosages, with the associated data indicating no trend between NR abundance and irradiation dose. The inoculation of the cork samples produced an increase in NR abundance. This current research effort focused on the characterization of these NRs. The radiation dosages were chosen based on current dosages used in commercial food irradiation practices.

2.2. Experimental Methods

Four types of typically-used corks were purchased from Juvenal Cork Inc. (Fairfield, CA) and labeled as follows: a high-grade natural cork (**A**), a secondary sample of natural cork (**B**), a composite cork contained within two slices of natural cork (**C**), and a composite cork (**D**). Cork type **C** was only examined from the inner composite piece. Composite corks are composed of ground natural grade cork combined with food-grade polyurethane glue. The microbial cultures *Paecilomyces viridis* (CECT 20427), *Paecilomyces glabrum* (CECT 20558), *Paecilomyces chrysogenum* (CECT 2306), *Mucor racemosus* (CECT 2670), *Trichoderma viride* (CECT 20721), *Aspergillusoryzae* (CECT 2095), *Cladosporium oxysporum* (CECT 20421), were received in dehydrated form from the Colección Española de Cultivos Tipo (CECT – Spanish Type Culture Collection). CECT 2306 was rehydrated with 0.3 ml of malt broth (Difco Sparks, MD), then propagated in 90 ml of malt broth at 24 °C for 72 hours. The remaining strains were each rehydrated with 0.3 ml of potato dextrose broth (Difco Sparks, MD), then propagated in 90 ml of potato dextrose broth at 24 °C for 72 hours. The cultures were transferred to sterile 15 ml centrifuge tubes and centrifuged at 2500 rpm for 10 minutes in a Beckman-Coulter centrifuge Model B4 (Winchester, VA). The supernatant was discarded, and the resulting pellets were re-suspended in 9.9 ml 0.85% sterile saline, vortexed, and re-centrifuged. This process was

completed twice before dispensing 0.5 ml of the resulting culture into 17 × 60 mm screw cap vials containing 4.5 ml 0.85% sterile saline. Aliquots of 1 ml from each culture were combined to make a microbial suspension in a sterile bottle containing 93 ml of 0.1% peptone water. The prepared inoculum, now containing each of the 7 TCA producing mold strains at a concentration of ca. 10^7 CFU/ml, was used within 2 hours after preparation and was kept at room temperature (23 °C to 24 °C) during the experiment.

2.2.1. Inoculation of Cork with Mold

One set of corks was investigated in an "as-purchased" condition (*vide supra*), and the second set was inoculated with the mixture of the molds, each known for their ability to convert TCP to TCA, allowing us to assess the effect of irradiation on mold-infected corks. Corks were inoculated aseptically with 1 cc of the mold solution injected into the center of each cork using a sterile 30 G 0.3 × 13 mm hypodermic needle (Allegiance, Mcgaw Park, IL). A new sterile needle was used for each cork. Using protocol established by Sadex Corporation, 10 g of inoculated corks were weighed out using a Mettler PM 480 balance (Columbus, OH) and placed into 80 ml VWR stomacher bags, then sealed using their flat wire closure. The 80 ml sealed stomacher bags containing inoculated corks were then placed together in a 1650 ml VWR stomacher bag. Each of the 1650 ml stomacher bags was folded over to the secure contents, and sealed using a vacuum sealer (FoodSaver model V2420; Providence, RI.) to minimize any cross-contamination risk during shipping.

2.2.2. Commercial Irradiation

Both sets of cork samples, *vide supra* and inoculated, were sent to Sadex Corporation, Sioux City, IA, an e-beam irradiation facility, for irradiation treatment with an average absorbed dose of 5, 10, and 15 kGy. High-density polyethylene sheets were used as attenuators to reduce

the energy of the incident electrons, resulting in the target dose. Additionally, a control set of each as-purchased and inoculated cork was sent to the Sadex Corporation facility, but did not receive any irradiation, to maintain consistent shipping and handling conditions among all the samples; these were labeled as 0 kGy.

2.2.3. Sample Preparation and Characterization of Corks after Irradiation

Figure 2.1 shows the flow diagram for the handling of cork samples upon their return from Sadex. Corks returning from Sadex were cut into disks and coated on one side with a thin gold layer to prevent surface charging while examining the surfaces via SEM and energy-dispersive x-ray spectroscopy (EDX). Upon confirmation of the presence of NRs by SEM, the NRs were isolated by sonicating cut pieces of non-inoculated SEM sample disks in ethanol (Pharmco-AAPER, Brookfield, CT), then centrifugation to ensure separation of the NRs from the cork before removing cork pieces from the ethanolic solution. Isolation of the NRs was needed because EDX and Raman spectroscopy were incapable of distinguishing between the cork and the embedded NR. The NRs dispersed in ethanol were characterized using transmission electron microscopy (TEM), EDX, and Raman spectroscopy. EDX samples were prepared by dropping NR/ethanol solution onto copper (Cu) tape. For the TEM analyses, the NRs were deposited on a 300 mesh holey carbon-coated copper grid. Raman samples were prepared by dropping NR/ethanol solution onto 4 mm fused silica glass disks. In all cases, data were collected after allowing ethanol to evaporate.

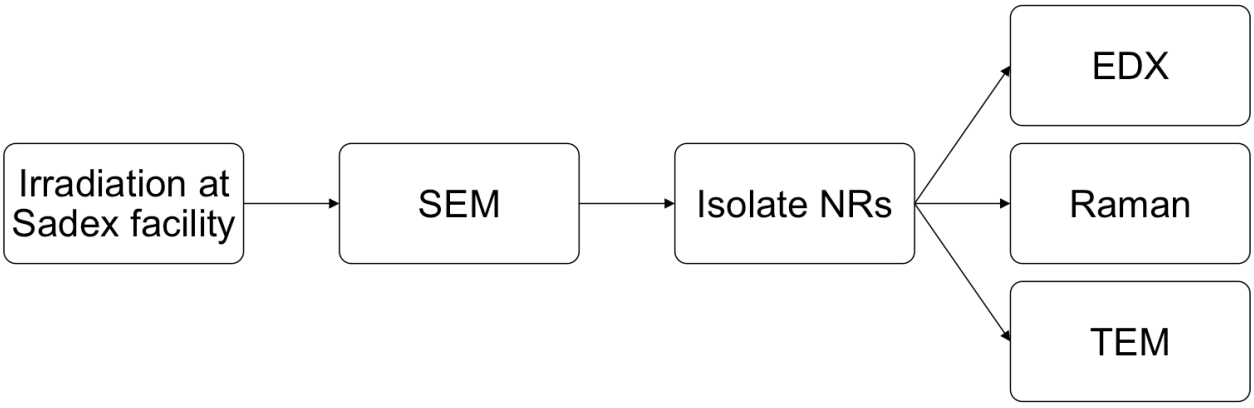

Figure 2.1. Procedural scheme for handling of cork samples returning from irradiation treatment at Sadex e-beam facility.

2.2.4. Instrumentation

Initial images of the commercially irradiated corks were obtained using a scanning electron microscope (LEO 1525 FE-SEM) using 15 kV e-beam. To prepare the samples for imaging, a gold coating was applied using a Polaron sputter coater. The NRs from the cork were isolated by sonication using a Misonix Sonicator S-4000 with a Microtip reaching a total of 2500 J of energy. Centrifugation between sonication steps was done using a VWR Clinical 50 Centrifuge operating at 4000 rpm for 10 minutes. EDX spectra were obtained using a JEOL JSM 6330F SEM with an EDX attachment using a 15 kV e-beam at a 15 mm working distance. TEM images were obtained with a JEOL 2000 FX TEM using a 200 kV e-beam. Raman spectra were obtained with a Horiba XploRA Spectrometer with a 532 nm laser and the following settings and parameters: 50% filter, 100 hole, 50 slit, 1200T grating, 0.5 s RTD exposure, 10 s exposure, and 2 accumulations. The spectra were smoothed once and baseline corrected with the smoothing and automatic baseline correction functions, respectively, using the LabSpec program. Controlled e-beam lithography (EBL) treatment was conducted in an FEI XL30 SEM

equipped with a lithography system, operating with a 5 kV e-beam and a 0.1 nA measured beam current. The beam was transmitted through a 30 μm aperture into a chamber where the pressure was maintained at 10^{-5} mBar.

2.2.5. Simulation of Commercial Irradiation via EBL

For EBL experiments, a new set of corks without previous irradiation treatment was obtained. For this purpose, we only used natural sample **B** and composite sample **D**. Cork samples were separated into two sets, *vide supra* and inoculated (prepared as described in Section 2.2.1). Cork samples were imaged using a 1 kV e-beam and then subjected to a 15 kV e-beam exposure from the SEM. With the scanning e-beam, images were captured every one minute until reaching a total of five minutes, then images were captured every five minutes until reaching a total of thirty minutes. An illustration of this time scheme can be seen in **Figure 2.2**. Additionally, a focused e-beam was applied where the e-beam was held stationary on one spot rather than scanning the entire image frame. A clean area of cork was imaged and focused using a 1 kV scanning e-beam, then changed to a 1 kV spot e-beam, followed by changing to a 5 kV spot e-beam, resulting in a beam of approximately 100 nm in diameter. After the designated time, the beam was switched from the 5 kV spot e-beam to a 1 kV spot e-beam, then changed to a 1 kV scanning e-beam to capture the image. Images were captured using the same time scheme as was used in the scanning e-beam experiments. Using the low voltage 1 kV e-beam throughout all captured images ensured that the imaging e-beam exposure was small relative to the irradiation e-beam exposure, and also allowed for all images to be of comparable resolution. This factor was especially important in the focused e-beam experiments, where the order of changing voltages and e-beam type was designed to minimize the imaging e-beam exposure.

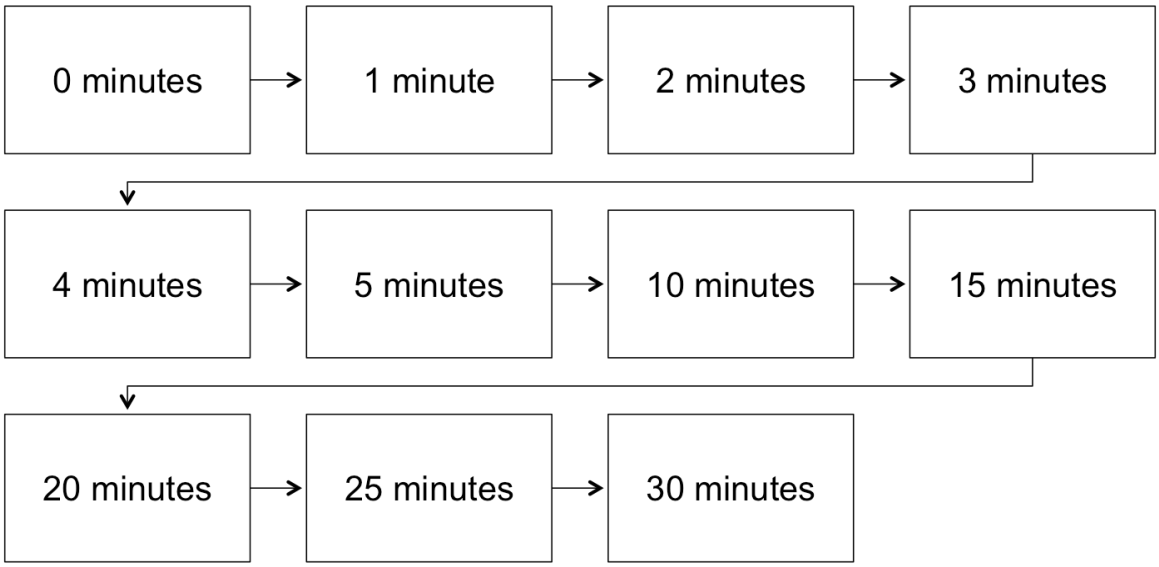

Figure 2.2. Images from EBL experiments were captured using the shown time scheme, every one minute until reaching a total of five minutes, then every five minutes until reaching a total of thirty minutes.

2.3. Results and Discussion

2.3.1. Analysis and Characterization

Both sets of *vide supra* and inoculated corks were examined by SEM to explore any changes that occurred from commercial e-beam irradiation exposure and to confirm the reduction or elimination of mold. As represented in **Figure 2.4**, all cork samples contained NRs. Interestingly, there were more NRs present inside the cork than on the outer surface of the cork, as seen in **Figure 2.3**, despite the low penetration depth of the e-beam relative to the other irradiation methods.

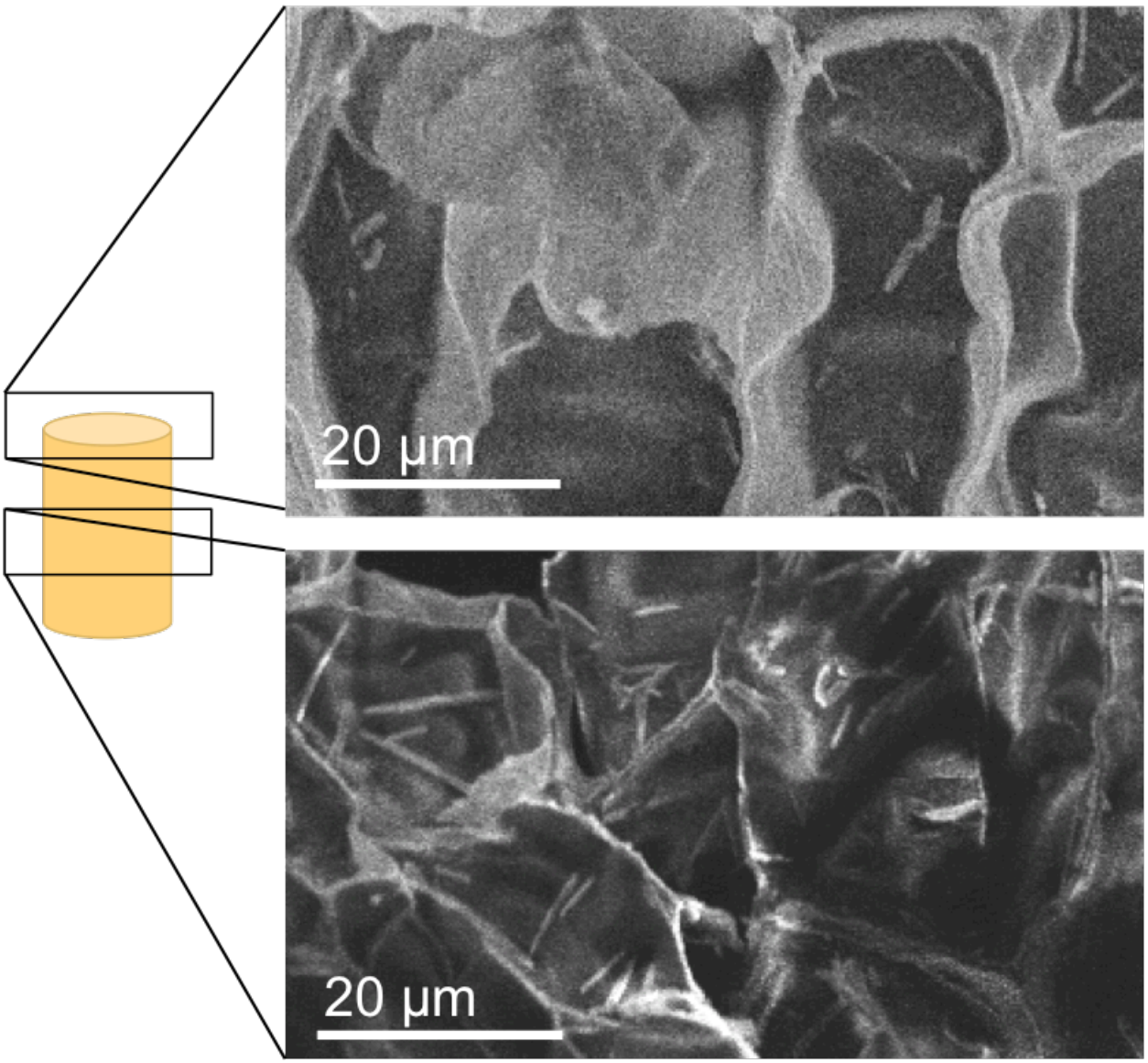

Figure 2.3. SEM micrographs of cork taken from the outer surface of the cork (top) and inside the cork (bottom).

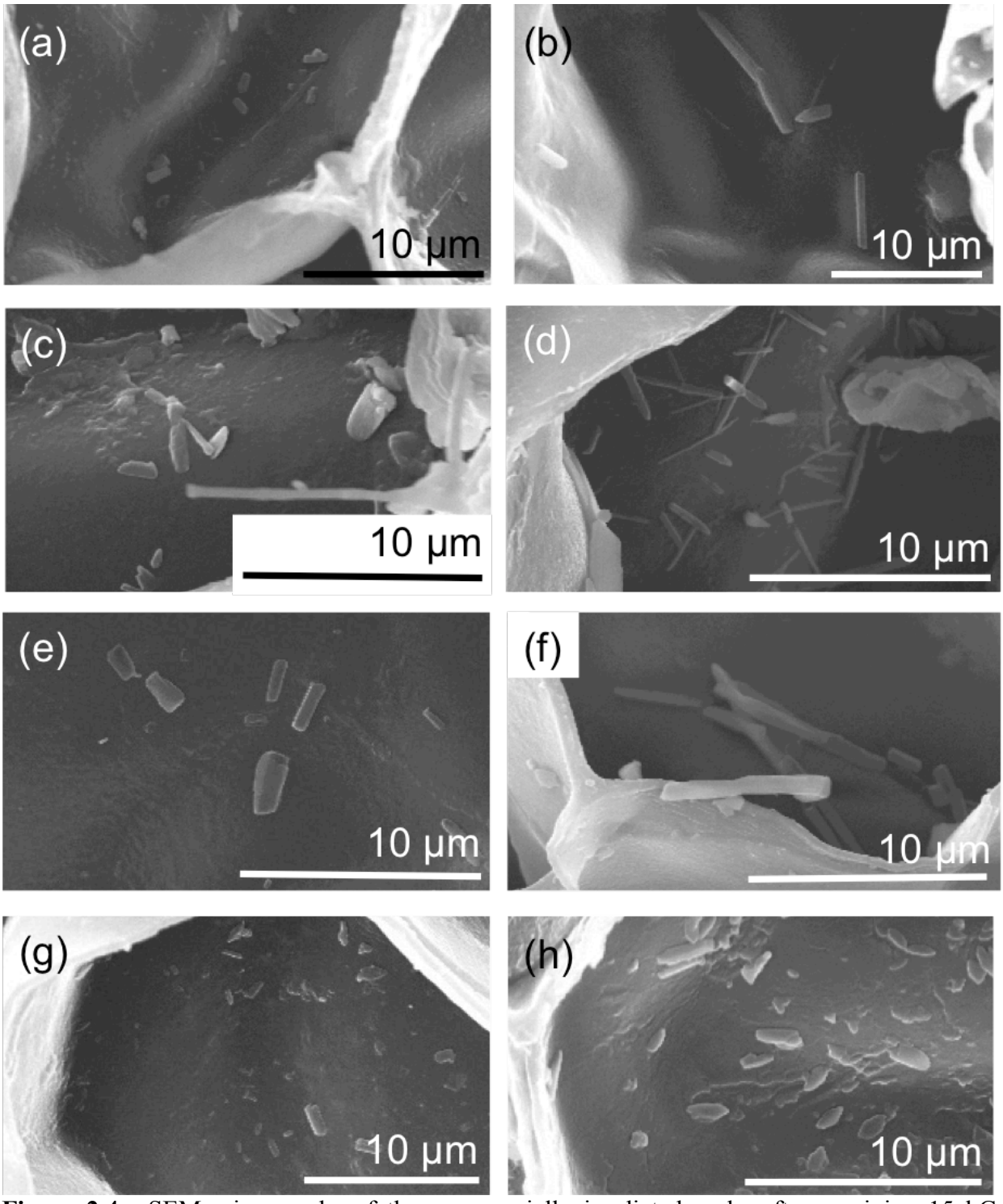

Figure 2.4. SEM micrographs of the commercially irradiated corks after receiving 15 kGy irradiation (a) type **A**, non-inoculated; (b) type **A**, inoculated; (c) type **B**, non-inoculated; (d) type **B**, inoculated; (e) type **C**, non-inoculated; (f) type **C**, inoculated; (g) type **D**, non-inoculated; (h) type **D**, inoculated, showing the presence of NRs throughout the cork sample.

The population density of the NRs formed from commercial e-beam irradiation was calculated from the total count from the SEM images divided by the total area, providing the number of NRs per unit area. The images shown here are for corks subjected to 15 kGy irradiation. The resulting data are provided in **Table 2.1**. In the case of the natural cork samples **A** and **B**, the NR population density increases from 0 kGy to 5 kGy, but does not continue on the same trend to 15 kGy. The composite cork samples **C** and **D** do not show a clear trend between NR abundance and absorbed radiation dose. The presence of NRs in non-irradiated samples **A**, **C**, and **D** prevents us from establishing a clear baseline from where we can say that commercial e-beam irradiation causes the formation of NRs. Also, as seen from samples absorbing 15 kGy radiation, the presence of mold resulted in an increased NR population compared to its non-inoculated counterpart.

Table 2.1. Population Density of NRs (count per μm^2)

		(# NRs/μm^2)/10^{-5}	
Cork type	kGy	As-purchased	Inoculated
A	0	54	--
	5	130	--
	15	5	68
B	0	0	--
	5	87	--
	15	43	280
C	0	190	--
	5	2	--
	15	0	17
D	0	110	--
	5	0	--
	15	28	42

Furthermore, imaging at higher magnification, seen in **Figure 2.5**, shows the NRs might be growing along the cork surface, from the cork cells, or from material below the cork surface.

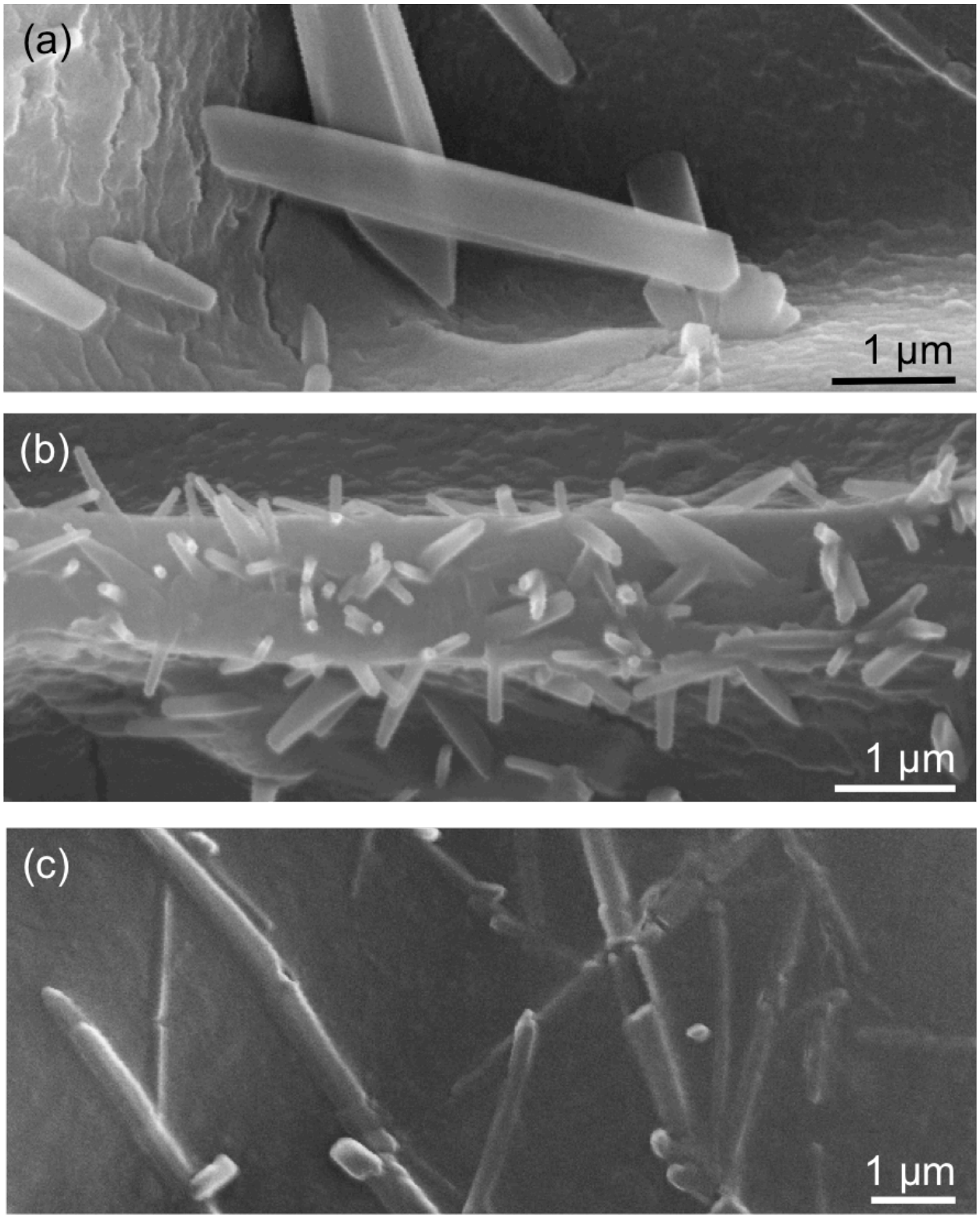

Figure 2.5. Imaging at higher magnifications shows NR formation may be occurring by growing (a) along the cork surface, (b) from the cork cells, or (c) from the material below the cork surface.

Chemical analysis by EDX of the isolated NRs from commercially irradiated natural and composite corks on Cu tape shows only the presence of carbon (C) and oxygen (O), as can be seen in **Figure 2.6**. The elements C and O are also present on the Cu tape, which can attributed to the e-beam penetrating through the Cu layer on the tape and down to the adhesive.

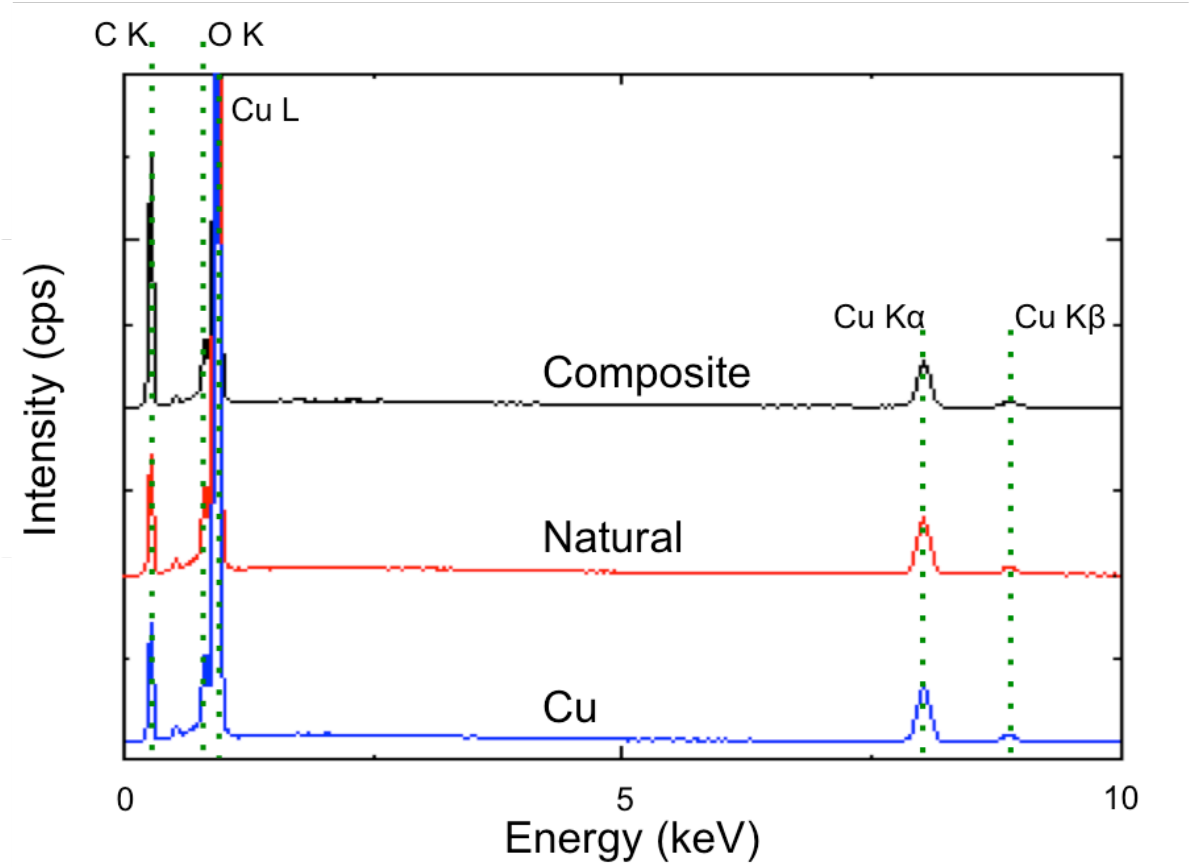

Figure 2.6. EDX spectra of NRs isolated from natural and composite cork on Cu tape showing the presence of C and O.

TEM was used to obtain higher-resolution images, allowing observation of the atomic structure of the NRs, as shown in **Figure 2.7**. The NRs found in commercially irradiated natural cork have a crystalline appearance, taking on a formation with an interlamellar spacing of approximately 0.96 nm. With carbon nanotubes (CNTs), a d-spacing of approximately 0.33 nm

occurs;[7-11] therefore, we conclude the structures from commercially irradiated natural cork are different from CNTs. Additionally, the NRs from commercially irradiated composite cork are seemingly amorphous. Alternatively, it is possible these NRs are really of chiral formation or the d-spacing is below the resolution of the microscope. The difference in crystallinity between the NRs from natural and composite cork most likely arises from the composition of the respective corks; the glue found in composite cork most likely contributes to the synthesis of the NRs in that cork.

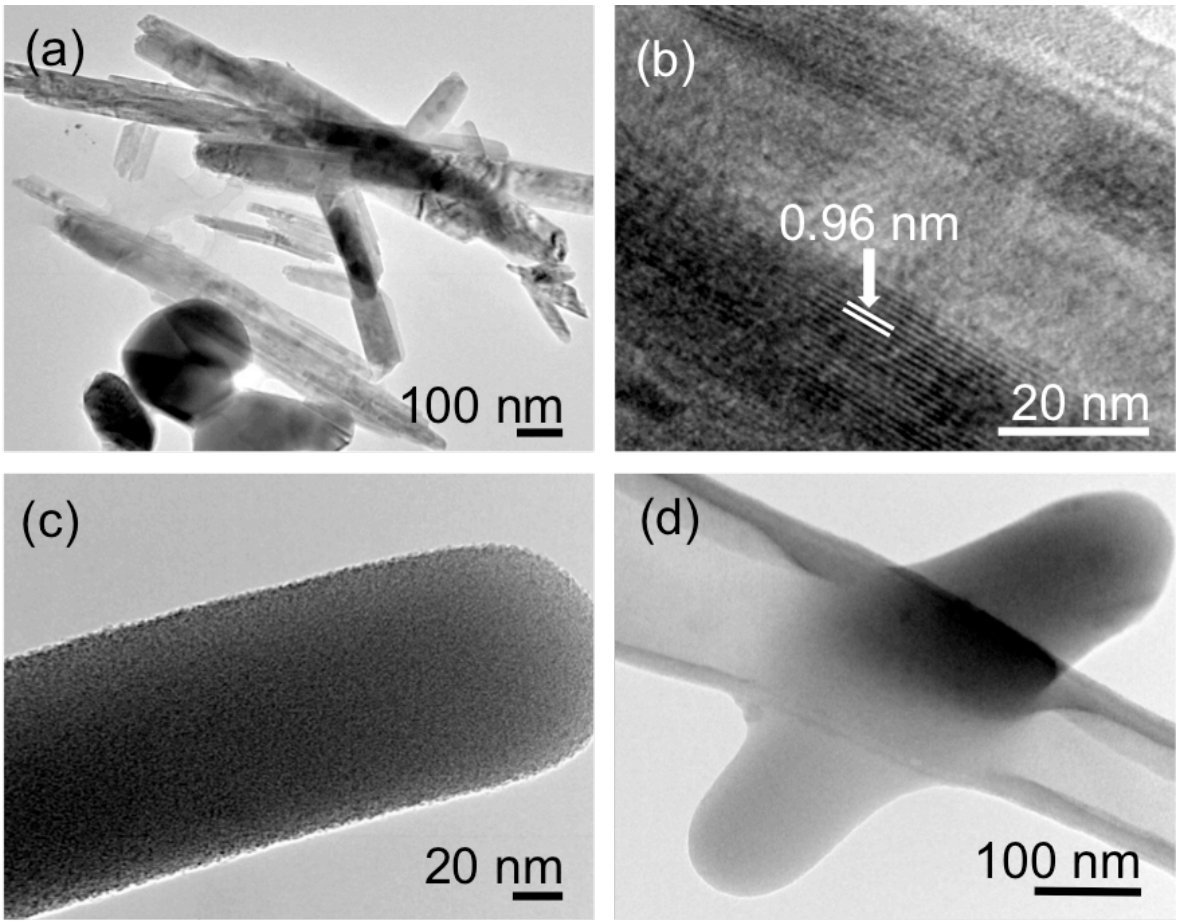

Figure 2.7. TEM micrographs of NRs isolated from (a) commercially irradiated natural non-inoculated cork, with close-up image (b), and (c) commercially irradiated composite non-inoculated cork, with close-up image (d), both irradiated to 5 kGy. Micrograph (b) shows interlamellar spacing of 0.96 nm, suggesting crystallinity in the structure.

Keeping in mind EDX found only the elements C and O, and assuming the presence of H, we conclude the NRs originated from cork components, namely lignin and cellulose,[12, 13] both organic compounds consisting of only C, hydrogen (H), and O. Raman spectra band assignments, **Figure 2.8** and **Table 2.2**, were proposed based upon those for lignin and cellulose.[14, 15] The fused silica glass shows a band at 445 cm^{-1}, and is thus present in all spectra as background.

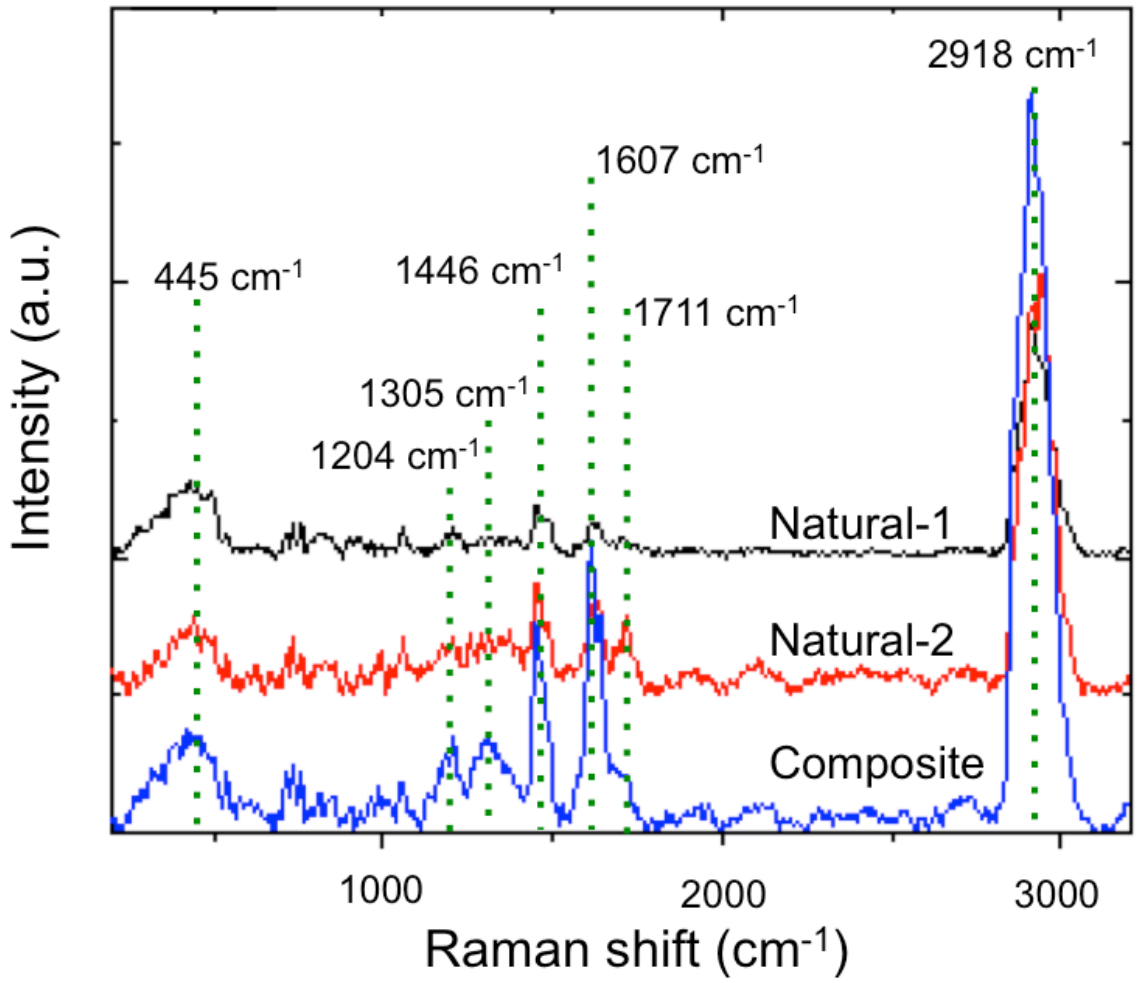

Figure 2.8. Raman spectra of the NRs isolated from non-inoculated natural and composite corks irradiated to 5 kGy. Two predominant spectra arose from the NRs found in natural cork, while NRs found in composite cork consistently provided the above spectrum.

Present in all three spectra are signals at 1446 and 2918 cm^{-1}, indicating HCH scissoring and CH stretching, respectively. As represented in **Figure 2.8**, two predominant spectra came from the collection of NRs from non-inoculated natural cork, differing in the presence of signal at 1204 and 1711 cm^{-1}, indicating OH bending and carbonyl CO stretching. Also, the spectra of NRs from non-inoculated composite corks exhibited a signal at 1305 cm^{-1}, indicating HCC and HCO bending. With the visual similarity of the NRs to CNTs, CNT Raman band assignments were also considered for this analysis.[16] The most characteristic Raman signal of CNTs is the G-band, which we propose is the signal at 1607 cm^{-1}. The G-band occurs from an optical phonon mode between two dissimilar carbon atoms, and can be seen in graphite, graphene, and CNTs. The signal at 1305 cm^{-1} in the composite cork sample, which we have already assigned as HCC and HCO bending seen in cellulose, can also be associated with the D-band of a CNT, sometimes referred to as the disorder-induced mode.

Table 2.2. Proposed Raman Band Assignments of NRs Isolated from Commercially Irradiated Corks

Natural-1	Natural-2	Composite	Proposed band assignment
1204		1204	OH bending
		1305	HCC bending, HCO bending, D-band
1446	1446	1446	HCH scissoring
1607	1607	1607	G-band
	1711		CO stretching
2918	2918	2918	CH stretching

2.3.2. Simulation of Commercial Irradiation via EBL

To confirm NR formation as a result of e-beam irradiation, *in situ* irradiation was performed using the e-beam of an SEM with lithography capabilities. This approach allowed for the observation of the cork surface during e-beam treatment, and prevented any external influence, such as shipment and worker handling of the samples, as was the case with our use of a commercial irradiation facility. For reasonable comparisons, we needed to replicate the absorbed radiation doses. One gray is defined as 1 kilogram of irradiated substance absorbing 1 joule of energy, presented in terms of joules per kilogram.[17] The components given from operation of the SEM can be combined to calculate energy absorbed, as shown in **Equation 2.1**:

$$Gy = \frac{E}{m} = \frac{C\,V}{m} = \frac{I\,V\,t}{m} \qquad (2.1)$$

where energy E is in joules (J), mass m of irradiated substance in kilograms (kg), electric charge C in Coulombs (C), voltage V in volts (V), current I in amperes (A), and time t in seconds (s). Using **Equation 2.1**, we calculated the time required for the 7 nm e-beam to scan a 2400 x 1800 μm^2 area for the scanning experiments and the 100 nm e-beam for stationary e-beam experiments to reach the specified absorbed radiation dosage, with the resulting data accumulated in **Table 2.3**.

Table 2.3. Radiation Dosage for E-Beam Scanning and Spot Experiments

Radiation dose (kGy)	Current (A)	Voltage (kV)	Mass (kg)	Time (s)
Scanning 2400 x 1800 μm^2 area with 7 nm diameter beam				
0	$1*10^{-10}$	5	$5*10^{-9}$	0
5	$1*10^{-10}$	5	$5*10^{-9}$	52
10	$1*10^{-10}$	5	$5*10^{-9}$	104
15	$1*10^{-10}$	5	$5*10^{-9}$	156
Single spot with 100 nm diameter beam				
0	$1*10^{-10}$	5	$9*10^{-18}$	0
5	$1*10^{-10}$	5	$9*10^{-18}$	$9*10^{-8}$
10	$1*10^{-10}$	5	$9*10^{-18}$	$2*10^{-7}$
15	$1*10^{-10}$	5	$9*10^{-18}$	$3*10^{-7}$

Figure 2.9 shows an example where NRs were successfully synthesized with the lithography system, while **Table 2.4** provides the tabulated percentages of successful NR formation from EBL on the cork samples.

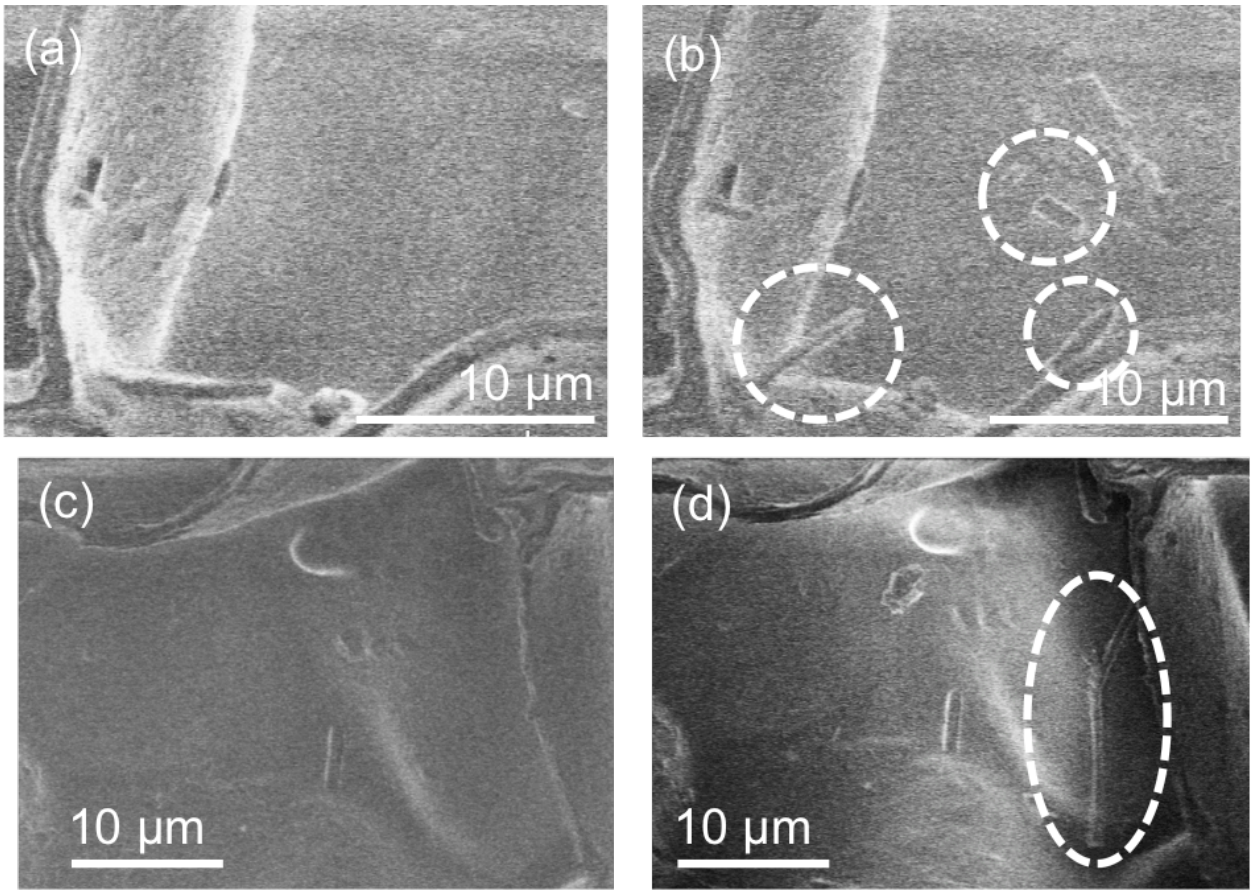

Figure 2.9. SEM micrographs of a non-inoculated, natural cork sample (a) before and (b) after 5 minutes exposure, and a separate non-inoculated, natural cork sample (c) before and (d) after 15 minutes exposure to the scanning e-beam of diameter 7 nm. The dashed line circles identify NRs synthesized using EBL.

Table 2.4. Success Rate of NR Synthesis in Cork Samples Irradiated via SEM E-Beam

	Trials showing NR formation	Total trials	Percentage trials showing NR formation
Scanning mode			
Natural, as-purchased	1	12	8%
Natural, inoculated	2	8	25%
Composite, as-purchased	2	8	25%
Composite, inoculated	3	5	60%
Spot mode			
Natural, as-purchased	0	7	0%
Natural, inoculated	0	6	0%
Composite, as-purchased	0	6	0%
Composite, inoculated	3	6	50%

The *in situ* synthesis of NR-laden corks by EBL demonstrates that commercial e-beam irradiation was indeed a likely source for NR formation in wine corks. It is important to note that NR formation occurred instantaneously during the switching between the imaging voltage of 1 kV to the irradiation voltage of 5 kV. For this study, longer exposure times had no apparent influence. As seen in **Table 2.3**, exposure to the SEM e-beam should have accumulated sufficient energy to reach the same absorbed radiation dose as was seen in the commercially irradiated cork samples; however, our lithography experiments did not reflect similar abundance of NRs. This discrepancy, we believe, comes from the operating energy of the incoming e-beam. Commercial e-beams, powered with linear accelerators, can provide 5-10 MeV energy, while the SEM (FEI XL30) e-beam can only operate at 5-30 kV. For perspective regarding this difference, **Equation 2.2** provides the relationship between energy and voltage:

$$E = VQ \tag{2.2}$$

where E is in electron-volts (eV), V in volts (V), and Q the elementary charge of one electron, equal to 1; in this case, eV and V are essentially equal. While the EBL experiments were designed for the sample to absorb the same energy over time, it appears that the energy from the incoming electrons is the determinant of NR formation; the electrons from commercial irradiation sources have a much higher energy than those coming from the SEM used in EBL experiments.

2.4. Conclusions

NRs were present in cork samples at all radiation dosages, even 0 kGy, preventing us from quantitatively confirming the effect of irradiation. The commercial e-beam treatment of corks produced data that showed corks inoculated with mold before e-beam treatment often contained more NRs than corks not inoculated before e-beam treatment. Analysis and characterization of NRs found in commercially irradiated wine corks showed the NRs were different from the CNTs we used as a nanomaterial reference. Similarities between CNTs and the NRs found in the commercially irradiated corks were the visual morphology, the presence of the characteristic D- and G-bands in the Raman spectra, and, in the case of NRs from commercially irradiated non-inoculated natural cork, molecular orientation, seen as crystallinity in TEM micrographs. The NRs were larger (micron-scale) as compared to the CNTs (usually nano-scale). Also, based on EDX analysis and proposed Raman band assignments, NRs contained O within the structure, whereas CNTs only contained C. The presence of glue in the composite cork samples may have also influenced the morphology and the overall crystallinity of the NRs. To simulate commercial e-beam treatment, we exposed non-irradiated cork samples to the SEM e-beam, and observed the formation of NRs in some instances. The inability to produce

NRs in all lithography trials likely comes from the difference in magnitude of energy of the incoming electrons, where the SEM e-beam is much weaker than the commercial e-beam.

2.5. Future Work

Additional data and multiple trials will help present a more robust conclusion about the effect of irradiation. For further crystallinity studies, powder x-ray diffraction (XRD) measurements can be made of powdered cork and NR samples. Specifically, XRD measurements on the NRs from composite cork can prove if the configuration is amorphous or chiral. Additionally, other *in situ* NR synthesis studies might be possible if the sample can be examined while at the commercial irradiation facility.

2.6. References

(1) The U.S. Food and Drug Administration Center for Food Safety and Applied Nutrition Food Information. Food Irradiation: What You Need to Know. *2014 Fact Sheet-Food Facts from the U.S. Food and Drug Administration*.

(2) U.S. Public Health Service, U.S. Department of Health and Human Services. Toxicological Profile for 2,4,6-Trichlorophenol. *Agency for Toxic Substances and Disease Registry*. 1990.

(3) Corsi, A.J. The Effectiveness of Electron Beam Irradiation to Significantly Reduce or Eliminate Molds Known to Cause 2,4,6-Trichloroanisole in Cork Stoppers. M.S. Thesis, University of Houston, Houston, TX, 2011.

(4) Magrez, A.; Kasas, S.; Salicio, V.; Pasquier, N.; Seo, J.W.; Celio, M.; Catsicas, S.; Schwaller, B.; Forro, L. Cellular Toxicity of Carbon-Based Nanomaterials. *Nano Lett.* **2006**, *6*, 1121-1125.

(5) Lanone, S.; Andujar, P.; Kermanizadeh, A.; Boczkowski, J. Determinants of carbon nanotube toxicity. *Adv. Drug Delivery Rev.* **2013**, *65*, 2063-2069.

(6) Mazzola, P.G.; Penna, T.C.V.; da S. Martins, A.M. Determination of decimal reduction time (D value) of chemical agents used in hospitals for disinfection purposes. *BMD Infect. Dis.* **2003**, *3*, 24-33.

(7) Fals, A.E.; Hadjiev, V.G.; Robles Hernández, F.C. Multi-functional fullerene soot/alumina composites with improved toughness and electrical conductivity. *Mater. Sci. Eng. A* **2012**, *558*, 13-20.

(8) Wang, Y.; Su, Z.; Wu, W.; Nie, S.; Lu, X.; Wang, H.; McCarty, K.; Pei, S.-S.; Robles Hernández, F.C.; Hadjiev, V.G.; Jiming, B. Anomalously Strong 2D Band Intensity in Twisted Bilayer Graphene: Raman Evidence for Doubly Degenerate Dirac Band. arXiv preprint arXiv:1309.5496, 2013.

(9) Geim, A.K.; Novoselov, K.S. The rise of graphene. *Nature Mater.* **2007**, *6*, 183-191.

(10) Novoselov, K.S.; Geim, A.K.; Morozov, S.V.; Jiang, D.; Zhang, Y.; Dubonos, S.V.; Grigorieva, I.V.; Firsov, A.A. Electric field effect in atomically thin carbom films. *Science* **2004**, *306*, 666-669.

(11) Kosnykin, D.V.; Higginbothan, A.L.; Sinitskii, A.; Lomeda, J.R.; Dimiev, A.; Price, B.K.; Tour, J.M. Longitudinal unzipping of carbon nanotubes to form graphene nanoribbons. *Nature* **2009**, *458*, 872-876.

(12) Pereira, H. Chemical composition and variability of cork from *Quercus suber L. Wood Sci. Technol.* **1988**, *22*, 211-218.

(13) Dharmadhikari, M. Wine Corks. *Vineyard and Vintage View* **1994**, *9*, 1-7.

(14) Wiley, J. H. Raman Spectra of Celluloses. Ph.D. Dissertation, The Institute of Paper Chemistry, Appleton, WI, **June 1986**.

(15) Szymańska-Chargot, M.; Cybulska, J.; Zdunek, A. Sensing the Structural Differences in Cellulose from Apple and Bacterial Cell Wall Materials by Raman and FT-IR Spectroscopy. *Sensors* **2011**, *11*, 5543-5560.

(16) Dresselhaus, M.S.; Dresselhaus, G.; Saito, R.; Jorio, A. Raman spectroscopy of carbon nanotubes. *Phys. Rep.* **2005**, *409*, 47.

(17) United States Nuclear Regulatory Commission. Units of radiation dose. NRC Regulation Title 10, Chapter I, of the *Code of Federal Regulations*.

Chapter III. Irradiation of Herbs and Flour

3.1. Introduction

The United States is a heavy consumer of imported herbs and spices,[1] but most consumers are unaware of the microbial load these herbs and spices carry. Contaminants can come from improper packaging and storage conditions, exposure of the products to soil, excreta of birds or rodents, and insects.[2] Contamination by insects can initiate infestation and deterioration, and that by microbes can induce spoilage or toxicity – leading to loss of marketability of the product in both cases. To address these concerns, many imported herbs and spices currently undergo ionizing irradiation and are labeled with the Radura symbol on their product packaging, while multi-ingredient foods containing irradiated seasonings are not required to provide this labeling – for example, dried basil in tomato sauce.[3] Ionizing irradiation is the preferred method because it is a cold process that does not interfere with the aroma and flavor, as can occur with steam or fumigation. Additionally, fumigants like methyl bromide, ethylene dibromide, and ethylene oxide leave chemical residues that are harmful to human health and the environment, and, for these reasons, have been phased out in many countries.[4-7] Most countries approve ionizing irradiation on herbs and spices to doses up to 10 kGy, and in the U.S. up to 30 kGy.[2]

While electrons have a shallow penetration depth relative to γ- and x-rays, they are useful in targeting small items, such as grains, prepackaged meats, herbs, and spices.[8] Van Calenberg *et al.* found electron beam (e-beam) irradiation to be effective in reducing or eliminating various molds and bacteria in white pepper, sweet paprika, and nutmeg with a study that analyzed the results from doses of 0, 2.5, 5, 7.5, and 10 kGy.[9] Their results showed greater reduction of the

number of coliforms, mesophilic bacteria, and thermophilic spores from larger irradiation dosages from both x-ray and e-beam. Also, storage of the irradiated spices did not indicate recovery of the microorganisms. Additionally, results from both x-ray and e-beam irradiation were comparable, such that one method was not more effective than the other. Another study focused on paprika found that while lower irradiation doses might be adequate for destroying the majority of the bioburden, 10 kGy was the recommended dose to provide optimum sanitation.[10] Their work determined the order of resistance to e-beam irradiation to be: coliform bacteria < molds and yeasts < sulfite-reducing clostridia. Dried chamomile inflorescences treated by e-beam showed a linear decrease in microbial load with absorbed radiation dose of 5 kGy.[11] Unfortunately, there was also a decrease in total content of flavonoids, tannins, and polyphenolcarboxylic acids, thus lowering the overall antioxidant activity of the chamomile plants. Additionally, Ramathilaga and Murugesan investigated effects of e-beam irradiation (doses up to 10 kGy) on an herbal mixture, chyavanaprash.[12] Chemical analysis found that only fat content increased with increasing irradiation dosage, while thiobarbituric acid reactive substances absorption, total phenolics, ferrous reducing power absorption, and gallic acid remained the same, regardless of irradiation dosage. Microbial analysis showed that bacterial and fungal counts reduced with irradiation treatments up to 7.5 kGy, above which the bacterial and fungal loads were fully absent.

In all the previous examples of investigations of the effect of e-beam irradiation upon the food product, the indicator of effectiveness was reduction in bacterial and fungal loads, as determined through colony plating. The goals of these prior studies were microbial safety, along with chemical and nutritional adequacy. Based on our experience during our efforts to analyze the effect of e-beam irradiation on cork samples (previous chapter), we decided to evaluate the

physical changes from e-beam treatment on selected dried herbs and wheat flour. Therefore, in this chapter, we report the results of our study of the effect of 1, 3, and 5 kGy doses of e-beam on herbs (basil, cilantro, oregano, and parsley) and flour. From our analysis of these irradiated food products using scanning electron microscopy (SEM) and e-beam lithography (EBL), we observed that both the dried herbs and flour developed nanostructures after commercial irradiation, while the EBL irradiated dried herbs and flour showed little to no indication of any change.

3.2. Experimental Methods

Fresh herbs (basil, cilantro, oregano, and parsley), typical of those entering the US market, were purchased from a local produce company. The herbs were dried by placing them in a commercial oven (HOBART Vulcan V36) at 167 °C for 30 minutes to reduce the water content in the leaf structure. Dried samples were labeled as follows: basil (**B**), cilantro (**C**), oregano (**R**), parsley (**P**). Non-irradiated, unbleached all-purpose flour (King Arthur brand) and irradiated, generic store brand (Safeway brand) unbleached all-purpose flour were obtained from a local grocery store. Flour samples were labeled as follows: King Arthur brand flour (**K**) and Safeway brand flour (**G**).

3.2.1. Simulation of Commercial Irradiation via EBL

Initial images of the herbs and flours, not previously irradiated, were obtained with a scanning electron microscope (FEI XL30 SEM) using a 1 kV e-beam, followed by controlled e-beam treatment with the instrument's lithography system. EBL experiments were separated into three types: 5 kV scanning e-beam, 15 kV scanning e-beam, and 15 kV focused spot e-beam. Scanning e-beams were of approximately 7 nm diameter while the focused spot e-beam was approximately 100 nm. Each EBL experiment operated with a 0.1 nA measured beam current

transmitted through a 30 μm aperture into a chamber where the pressure was maintained at 10^{-5} mBar. Scanning experiments began with finding a clean surface on the herb under examination, an area free of any nanostructures, initially using a 1 kV scanning e-beam, then changing the beam to the desired voltage, either 5 or 15 kV, and programming the beam to scan over the entire area in the micrograph. Micrographs were captured while using the exposure voltage every 1 minute up to 5 total minutes, then every 5 minutes up to 15 total minutes. The focused spot e-beam experiments also started with finding a clean surface on the herb under examination while using a 1 kV scanning e-beam. Next, the beam was changed to a 1 kV spot e-beam, followed by changing to a 15 kV spot e-beam, resulting in a beam of approximately 100 nm in diameter. After reaching the desired time of e-beam exposure, micrographs were captured by reverting from the 15 kV spot e-beam back to a 1 kV spot e-beam. Then images were collected using a 1 kV scanning e-beam, that is, the reverse procedure to exposing the sample to the focused e-beam. Captured micrographs were on the same time scale as that used in scanning e-beam experiments. By capturing all micrographs using the 1 kV e-beam, we ensured that the imaging e-beam exposure is small relative to irradiation e-beam exposure, while allowing for all images to be of comparable image resolution. This was especially important in focused e-beam treatments since the interaction of e-beam and material produces the SEM micrograph, the order of changing voltages and e-beam type was designed to keep the imaging e-beam exposure to a minimum and provide minimal impact upon the results associated with the e-beam irradiation experiments.

3.2.2. Commercial Irradiation

All herb samples, **B**, **C**, **R**, and **P**, and the flour sample **K** were sent to an e-beam irradiation facility (Sadex Corporation, Sioux, City, IA) for irradiation treatment. Average doses of 1, 3, and 5 kGy were chosen based upon recommendations from Sadex staff regarding current

allowed dosages in commercial food irradiation on herbs and spices. High-density polyethylene (HDPE) sheets were used as attenuators to reduce the energy of the incident electrons, resulting in the target dose. Additionally, a control set of each sample type was sent to the e-beam irradiation facility to replicate handling and shipment conditions, but this set of samples was not exposed to any radiation (labeled as 0 kGy). Upon return from Sadex, all samples were secured to specimen stubs by graphite tape and examined with our SEM using a 1 kV e-beam with a 0.1 nA measured beam current transmitted through a 30 μm aperture into a chamber where the pressure was maintained at 10^{-5} mBar.

3.3. Results and Discussion

In designing the lithography experiments, we chose a time-based approach, rather than accumulate the same absorbed dose as those used in commercial practices, to highlight the differences in the energy from the incoming electrons, whether or not the samples absorb the same total radiation dose between commercial and lithography e-beam exposures. In the case of e-beam irradiation of cork samples, the commercially irradiated corks consistently contained many nanorods (NRs), while the lithography irradiated corks showed NR formation only in some instances. The discrepancy in the abundance of NRs between the two irradiation methods, we believe, lies in the energy of the incoming electrons; commercial e-beams are powered by linear accelerators capable of accelerating electrons in a vacuum tube to several million volts,[13] while the SEM EBL system is limited to approximately 30 kV. This estimated limit can be used to derive the energy associated with the e-beam electrons using **Equation 3.1**, which relates energy and voltage,

$$E = VQ \tag{3.1}$$

where energy E is in electron-volts (eV), voltage V in volts (V), and the elementary charge of one electron Q equals 1. Therefore, the energy of the electrons generated by the commercial e-beam linear accelerators can reach up to 10 MeV while SEM can reach ~30 keV, resulting in a difference of three orders of magnitude in the energy associated with the individual electrons. Since the incoming energy from the two irradiation methods is not the same, it is possible that the 10 MeV electrons used in commercial irradiation is more than sufficient to reach the activation energy for NR-formation, while the 30 keV electrons from the SEM provide only enough energy for the NR-formation activation energy if all other factors are perfectly aligned.

Initial images of all non-irradiated herbs, basil, cilantro, oregano, and parsley showed no indications of the presence of nanostructures, prompting our controlled e-beam exposure by EBL experiments. As with the previous EBL experiments on corks that produced a small number of nanostructures in some samples, we wanted to see if EBL on the herbs could produce similar results. Lithography by scanning e-beam utilizing both 5 and 15 kV settings did not produce any effects on the dried basil leaves, while the focused spot 15 kV e-beam is shown to have damaged, possibly by burning, the dried basil leaf surface (**Figure 3.1**).

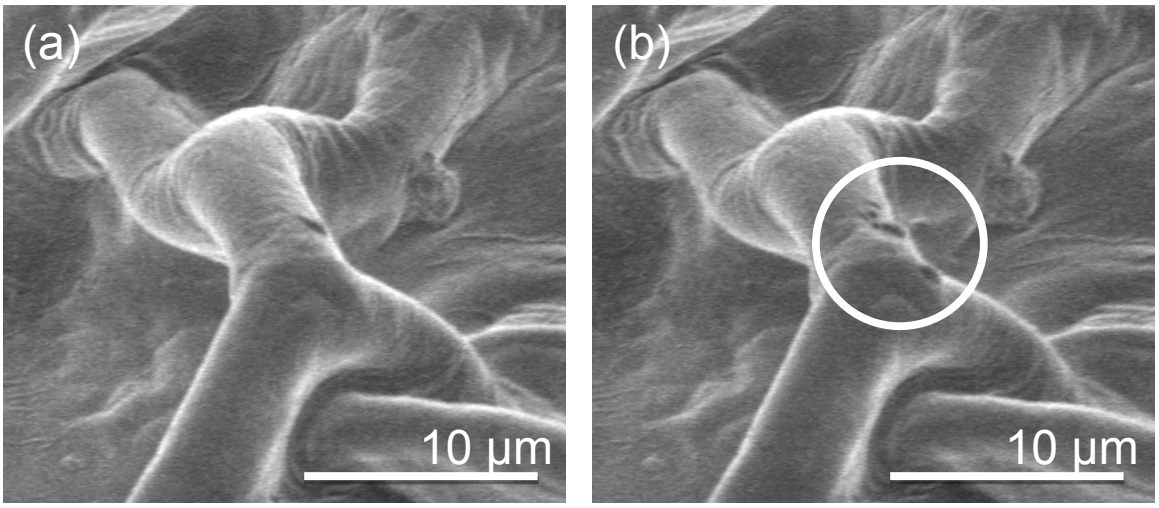

Figure 3.1. SEM micrographs of basil from focused 15 kV e-beam spot treatment recorded at (a) 0 and (b) 10 minutes of exposure, highlighting the damage caused by focused e-beam exposure.

In the case of lithography on dried cilantro, the scanning 5 kV e-beam also did not appear to have any effect on the surface of the leaf. Increasing the voltage of the scanning e-beam to 15 kV produced small particles in some samples, as shown in **Figure 3.2**. Similar to the case of dried basil, focused e-beam spot treatment caused damage to the cilantro leaf surface and stoma (**Figure 3.2**). Neither treatment (scanning or focused e-beam) appeared to produce any physical change, in the form of formation of new particles or damage to the respective dried leaf surface, to oregano or parsley.

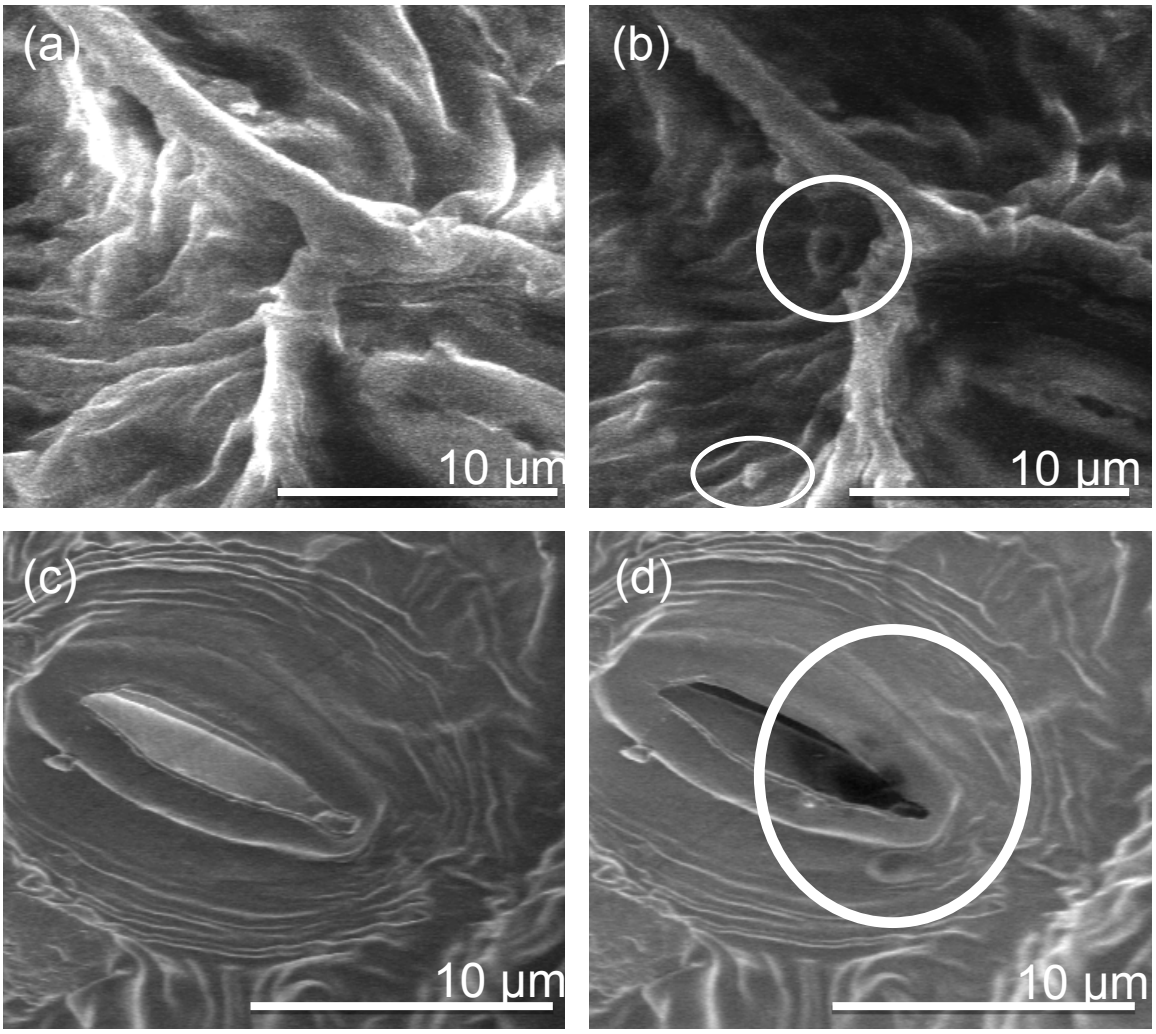

Figure 3.2. Dried cilantro exposed to the 15 kV scanning e-beam after (a) 0 and (b) 15 minutes, and to the 15 kV focused spot e-beam after (c) 0 and (d) 10 minutes. Scanning the area with the e-beam reveals the formation of small particles, as seen in (b), while the focused e-beam is shown to cause damage to the surface and stoma of the leaf, as seen in (d).

As discussed in the lithography experiments of the dried herbs using the scanning e-beam, the 5 kV e-beam did not provide sufficient energy to activate formation of particles, while, in the case of cilantro, the 15 kV scanning e-beam was capable of activating some particle formation. Since the 15 kV e-beam was able to activate nanostructure formation in the cilantro, we anticipate that commercial e-beam irradiation also activates nanostructure formation, since it has more incoming energy. The focused 15 kV e-beam did not induce any new particle formation, and actually appeared to damage the surface of basil and cilantro. The lack of new

particle formation from the focused 15 kV e-beam is similar to the focused e-beam treatment on cork, which also failed to produce new nanostructures. Since the focused e-beam is only about 100 nm in diameter, compared to the e-beam large enough to scan cases of foods in the commercial setting, there is only minimal exposure of the herb samples to the e-beam from lithography. It is possible that in having different beam sizes, the electrons are delocalized as a function of beam size, where the delocalization is greater in cases of large beam size, while the electrons are more localized in cases of small beam size. As observed in focused e-beam treatments, the flow of electrons is concentrated to a small area, where, rather than activating nanostructure formation, the high-energy electrons damage the target surface. In contrast, scanning EBL experiments have the electrons delocalized over a larger area than focused spot EBL, so the dispersion of electrons do not overload the target surface, and can prompt nanostructure formation. The delocalization of electrons can possibly extend even further to commercial irradiation treatment, where the electrons are even more delocalized to an even larger area and we expect to see even more nanostructure formation.

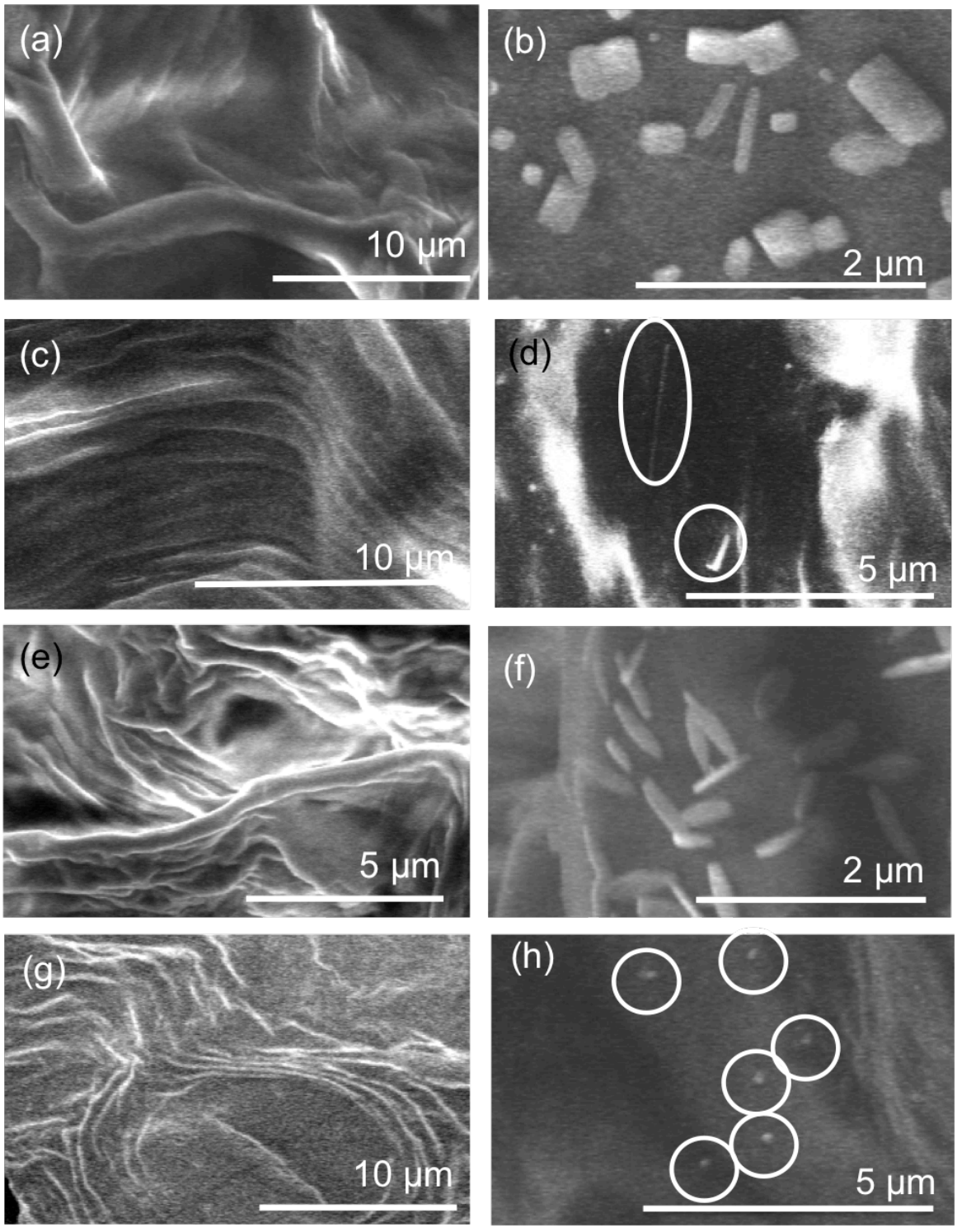

Figure 3.3. SEM micrographs of basil (a) non-irradiated and (b) irradiated, cilantro (c) non-irradiated and (d) irradiated, oregano (e) non-irradiated and (f) irradiated, and parlsey (g) non-irradiated and (h) irradiated by Sadex Corporation to 1 kGy. Nanostructures found on each type of leaf can be characterized in terms of morphology as (b) cubic with some rods, (d) rod-shaped, (f) grain-shaped, and (h) irregular spheres.

Since the lithography experiments were able to produce nanostructures on some of the samples, we proceeded with commercially irradiating all the herb samples, **B**, **C**, **R**, and **P**. Upon review, we found that nanostructures were present in all of the commercially irradiated samples, with varying morphologies depending on the herb leaf involved (**Figure 3.3**). In contrast, nanostructures were completely absent from the non-irradiated herb samples. For the commercially irradiated herbs, there were varying levels of abundance of the nanostructures, as shown with the nanostructure population densities in **Table 3.1**. The values in this table were calculated from the total number of nanostructures from all of the SEM micrographs of the commercially irradiated herbs divided by the sum of the areas of the respective micrographs. The most surprising result from these calculations is the abundance of nanostructures on the dried cilantro; e-beam lithography on cilantro showed the formation of a few particles, while lithography on the other herbs did not show nanostructure formation, indicating nanostructures forming on cilantro required a lower activation energy than the other herbs studied. However, cilantro contained the least amount of nanostructures after commercial irradiation, implying the activation energy of nanostructure formation on cilantro is greatest in the herbs studied. It is apparent with all of the herb samples that the abundance of nanostructures was greatest from the sample commercially irradiated to 1 kGy, while higher irradiation dosages resulted in fewer nanostructures. We postulate that the nanostructures most readily form starting with exposure to a threshold energy, or activation energy, while higher energies can cause an entirely different reaction from nanostructure formation. In the case of herbs, the energy limit before there is no longer nanostructure formation seems to be from absorption between 1 and 3 kGy.

Table 3.1. Population Density of Nanostructures in the Selected Herbs (count per μm^2)

Herb type	Absorbed radiation dose (kGy)	(# nanostructures/μm^2)/10^{-3}
Basil	1	35
	3	1.9
	5	1.1
Cilantro	1	1.5
	3	0
	5	0
Oregano	1	30
	3	0
	5	2.2
Parsley	1	48
	3	0
	5	0

As mentioned in experimental methods, the target dose was achieved using HDPE sheets, where samples requiring low doses would be irradiated by lower-energy electrons, and samples requiring high doses would be irradiated by higher-energy electrons. In the selected herbs, the energy from the electrons designed to provide 1 kGy absorbed dose provided the best conditions from those tested to have nanostructure formation. Electrons with higher energies, seen as higher absorbed doses, did not seem to induce nanostructure formation, and may have resulted in other reactions besides nanostructure formation.

Non-irradiated flour also did not contain any nanostructures. EBL experiments on flour, using both scanning and focused spot e-beam treatment, did not result in the formation of any new particles. SEM micrographs of generic store brand flour **G**, known to already have received irradiation before purchase in store, also lacked the presence of nanostructures. However, the commercial irradiation of **K** resulted in formation of nanorods when the sample absorbed 3 kGy

of radiation, as seen in **Figure 3.4**, with these nanostructures exhibiting a morphology similar to that found with those on the commercially irradiated corks.

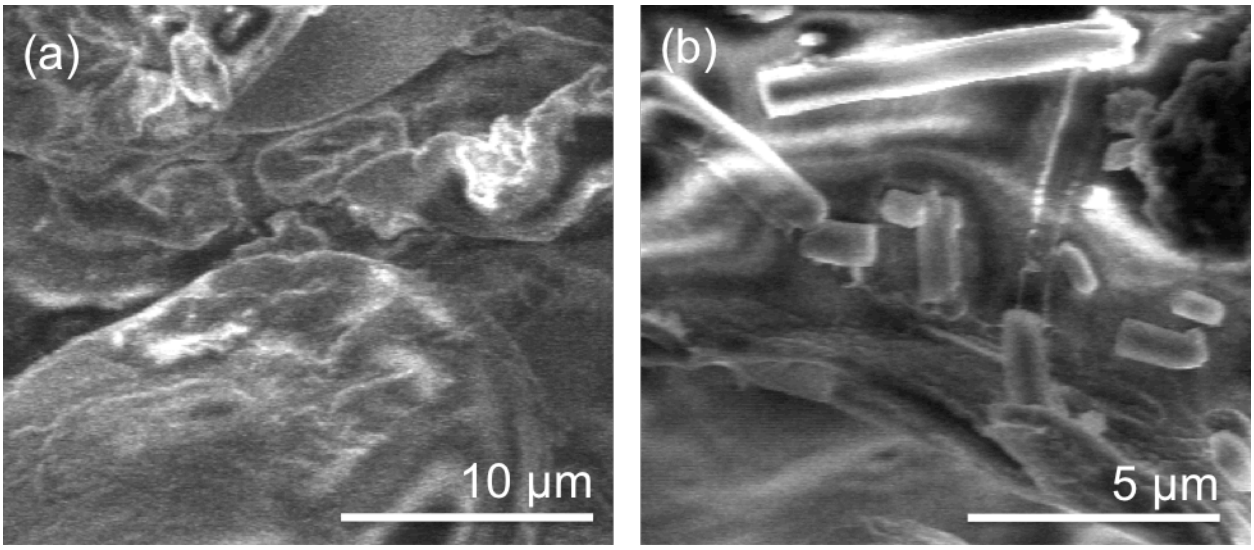

Figure 3.4. SEM micrograph of (a) a non-irradiated flour sample with no nanostructures, and (b) a separate flour sample irradiated by Sadex to 3 kGy, showing the presence of nanorods.

Nanorods, or other nanostructures, were completely absent from the non-irradiated flour samples and commercially irradiated flour samples absorbing 1 and 5 kGy irradiation (**Table 3.2**). We can use the same explanation from the irradiation of herbs regarding the abundance of nanostructures at various absorbed radiation dosages: a threshold energy must be received before the nanostructures will begin to form; however, higher energies might lead to a completely different reaction. In the instance of commercial irradiation of flour, the threshold energy appears to be from the energy designed for the target to absorb 3 kGy, and the maximum energy before nanostructures do not form is between the energy from absorbing 3 and 5 kGy.

Table 3.2. Population Density of Nanostructures in Flour (count per μm^2)

Absorbed radiation dose (kGy)	(# nanostructures/μm^2)/10^{-3}
1	0
3	23
5	0

3.4. Conclusions

Similar to the case of the cork stoppers, commercial e-beam irradiation of the selected herbs and flour samples promoted nanostructure growth on the surface of each irradiated food product. Lithography by an e-beam from SEM, while it does not provide the same level of energy relative to commercial e-beams, was capable of inducing the formation of nanostructures in a few instances. Noting that the previously-irradiated-store-bought flour sample contained no nanostructures, while the commercial e-beam irradiation led to the formation of nanostructures in samples irradiated to 3 kGy; the morphology of the observed nanostructures varied among the different irradiated products. The difference in the ability to produce nanostructures from each irradiation method is likely a function of the incoming e-beam energy. Commercial e-beam irradiation occurs at much higher energy as compared to SEM e-beams. The activation energy to efficiently form the nanostructures is possibly higher than the SEM e-beam energy and less than the energy of commercial irradiation. Thus EBL did not consistently show nanostructure formation on the irradiated food surface, while commercial irradiation did consistently produce nanostructures, but at e-beam exposures that appear to be dependent upon the food product involved and the nature of the exposure. The absorbed energy (dose) that was associated with the highest formation of nanostructures was ~1 kGy for selected dried herbs and ~3 kGy for flour. Also, there appeared to be a maximum absorbed energy for all the selected dried herb

samples and flour beyond which nanostructures do not form, as determined by a decrease in abundance of nanostructures. This maximum absorbed energy seems to be between 1 and 3 kGy in the selected dried herbs and between 3 and 5 kGy in flour.

This is the first report that demonstrates the presence of nanostructures after irradiation of selected food products. Similar nanostructures have long been under investigation for potential applications, including clinical biomedical applications.[14, 15] However, studies on the introduction of carbon nanotubes into the body, namely through pulmonary toxicity studies, have shown the possibility of cell apoptosis, necrosis, DNA damage, and cell death.[16] It remains uncertain how the nanostructures found with this investigation might affect the workers in a commercial irradiation facility or consumers of the selected irradiated products.

3.5. Future Work

To accurately determine the nanostructure activation energy and maximum absorbed energy beyond which nanostructures do not form, further studies, using a narrow window of radiation dosage, are warranted. Alternatively, the activation energy can be calculated from a set of experiments using the Arrhenius equation, shown in **Equation 3.2**

$$k = Ae^{\frac{-E_a}{RT}} \tag{3.2}$$

where k is the rate constant of the reaction, A is the Arrhenius constant, E_a is the activation energy, R is the universal gas constant, and T is the absolute temperature. The resulting plot of $ln(k)$ versus T^{-1} will give a straight line, where the activation energy can be defined as $-R$ times the slope of the Arrhenius plot, given constant pressure P, expressed as **Equation 3.3**.

$$E_a = -R\left(\frac{\partial lnk}{\partial \frac{1}{T}}\right)_P \tag{3.3}$$

Additionally, the nanostructures should be isolated from the food products and characterized by energy-dispersive X-ray spectroscopy (EDX), Raman spectroscopy, and X-ray diffraction measurements. Also, cytotoxicity testing of the nanostructures on cells, similar to cytotoxicity studies of carbon nanotubes, would be useful in determining possible health risks associated with the nanostructures formed from the selected irradiated food products. Previous studies on the effects of eating irradiated food products defined the well being of the test subjects through measurements including growth rate and studies on hematology, histopathology, and reproduction of the test subjects.[17-20] While those studies focused on the health of the test subject in a broad sense, cytotoxicity tests would allow for a fundamental determination regarding the biocompatibility of the nanostructures found during this investigation.

3.6. References

(1) Buzzanell, P.J.; Dull, R.; Gray, F. The Spice Market in the United States: Recent Developments and Prospects. *Agriculture Information Bulletin Number 709* U.S. Department of Agriculture, **1995**.

(2) Peter, K.V., *Handbook of herbs and spices, Vol. 3*. CRC Press: Boca Raton, FL, **2006**.

(3) Food Irradiation: What You Need to Know. *Food Facts From the U.S. Food and Drug Administration*, **2014**.

(4) Article 2H: Methyl bromide. *Handbook for the Montral Protocol on Substances that Deplete the Ozone Layer, 7E*. Secretariat of The Vienna Convention for the Protection of the Ozone Layer & The Montreal Protocol on Substances that Deplete the Ozone Layer: Nairobi, Kenya, **2006**.

(5) Agency for Toxic Substances and Disease Registrys (ATSDR). *Toxicologial Profile for 1,2-Dibromoethane*. Public Health Service, US Department of Health and Human Services: Atlanta, GA, **1992**.

(6) U.S. Environmental Protection Agency. *Integrated Risk Information System (IRIS) on 1,2-Dibromoethane*. National Center for Environmental Assessment, Office of Research and Development: Washington, DC. **1999**.

(7) ATSDR. *Toxicological Profile for Ethylene Oxide*. US Public Health Service, US Department of Health and Human Services: Atlanta, GA, **1990**.

(8) Radomyski, T.; Murano, E.A.; Olson, D.G.; Murano, P.S. Elimination of Pathogens of Significance in Food by Low-dose Irradiation: A Review. *J. Food Prot.* **1994**, *57*, 73-86.

(9) Van Calenberg, S.; Vanhaelewyn, G.; Van Cleemput, O.; Callens, F.; Mondelaers, W.; Huyghebaert, A. Comparison of the Effect of X-ray and Electron Beam Irradiation on Some Selected Spices. *Lebensm.-Wiss. Technol.* **1998**, *31*, 252-258.

(10) Nieto-Sandoval, J.M.; Almela, L.; Fernández-López, J.A.; Muñoz, J.A. Effect of Electron Beam Irradiation on Color and Microbial Bioburden of Red Paprika. *J. Food Prot.* **2000**, *63*, 633-637.

(11) Nemțanu, M.R.; Kikuchi, I.S.; de Jesus Andreoli Pinto, T.; Mazilu, E.; Setnic, S.; Bucur, M.; Duliu, O.G.; Meltzer, V.; Pincu, E. Electron beam irradiation of *Matricaria chamomilla* L. for microbial decontamination. *Nucl. Instr. and Meth. in Phys. Res. B* **2008**, *266*, 2520-2523.

(12) Ramathilaga, A.; Murugesan, A.G. Effect of electron beam irradiation on proximate, microbiological sensory characteristics of chyavanaprash—Ayurvedic poly herbal formation. *Innov. Food Sci. Emerg. Technol.* **2001**, *12*, 515-518.

(13) Fairand, B.P., *Radiation Sterilization for Health Care Products: X-Ray, Gamma, and Electron Beam*. CRC Press: Boca Raton, FL, **2001**.

(14) Colombo, M.; Carregal-Romero, S.; Casula, M.F.; Gutierez, L.; Morales, M.P.; Bohm, I.B.; Heverhagen, J.T.; D., P.; Parak, W.J. Biological applications of magnetic nanoparticles. *Chem. Soc. Rev.* **2012**, *41*, 4306-4334.

(15) Singamaneni, S.; Bliznyuk, V.N.; Binek, C.; Tsymbal, E.Y. Magnetic nanoparticles: recent advances in synthesis, self-assembly and applications. *J. Mater. Chem.* **2011**, *21*, 16819-16845.

(16) Nerl, H.C.; Cheng, C.; Goode, A.E.; Bergin, S.D.; Lich, B.; Gass, M.; Porter, A.E. Imaging methods for determining uptake and toxicity of carbon nanotubes in vitro and in vivo. *Nanomedicine (London, U. K.)* **2011**, *6*, 849-865.

(17) Read, M.S.; Trabosh, H.M.; Worth, W.S.; Kraybill, H.F.; Witt, N.F. Short-Term Rat-Feeding Studies with Gamma-Irradiated Food Products. *Toxicol. Appl. Pharm.* **1959**, *1*, 417-425.

(18) Bubl, E.C.; Butts, J.S. The Growth, Breeding and Longevity of Rats Fed Irradiated or Non-Irradiated Pork. *J. Nutr.* **1960**, *70*, 211-218.

(19) Burns, C.H.; Abrams, G.D.; Brownell, L.E. Growth, Reproduction, Mortality, and Pathologic Changes in Rats Fed Gamma-Irradiated Potatoes. *Toxicol. Appl. Pharm.* **1960**, *2*, 111-131.

(20) Tinsley, I.J.; Bone, J.F.; Bubl, E.C. The Growth, Reproduction, Longevity, and Histopathology of Rats Fed Gamma-Irradiated Peaches. *Toxicol. Appl. Pharm.* **1963**, *5*, 464-477.

Chapter IV. Conclusions and Future Work

4.1. Conclusions

My thesis focused on the formation of nanostructures after irradiation treatment; I evaluated their presence in food and related products, namely cork stoppers, basil, cilantro, oregano, parsley, and flour. There is a plethora of information on the microbiological safety and nutritional adequacy for food products after irradiation; however, formation of nanostructures, and their potential adverse health effects, has not been studied. These investigations have also provided useful information regarding the parameters that lead to nanostructure formation, which can be extended to other e-beam irradiated food products and will generate awareness of the possible presence of nanostructures in many irradiated foods.

In Chapter 1, I gave an overview on ionizing radiation, outlined its sources and mechanism of action, and then focused on the potential toxicological concerns of carbon-based nanomaterials. While irradiation treatment achieved the goal of microbiological safety in all the studies mentioned in Chapter 1, I chose to build upon the study that resulted in the formation of small protruding fibers resembling carbon nanotubes (CNTs) on irradiated corks. Similar effects on other irradiated food or non-food products have not been studied. The research presented in the next two chapters focused on the effect of irradiation on corks, selected spices, and flour.

In Chapter 2, I focused on identifying the nanostructures found in commercially irradiated wine corks, "as purchased" corks, and corks inoculated with mold, and demonstrated that e-beam irradiation of cork stoppers led to the formation of nanorods (NR) within the cork cavities. Evaluation of NR morphology concluded that abundance trends were a function of cork type (natural cork or composite cork). This investigation confirmed that the irradiation of cork

products can lead to the formation of nanostructures; however, the data failed to produce any clear correlation between the level of exposure to ionizing energy and the formation of nanostructures. The results obtained from this work were compared to the known properties of CNTs, and confirmed the NRs were of very different composition than CNTs.

To determine if the formation of nanostructures under irradiation is limited to the cork products, we studied other food products already approved for irradiation treatments. With herbs and spices, most countries already approve irradiation doses up to 10 kGy, and the United States up to 30 kGy.[1] However, any information on the effect of these exposures with respect to formation of nanostructures after irradiation is sorely lacking. Therefore, in Chapter 3, I studied the physical effects of e-beam irradiation on selected dried herbs, basil, cilantro, oregano, and parsley, along with flour, and demonstrated the presence of nanostructures on several of the food product surfaces after irradiation. The nanostructure morphologies varied among the different sample types.

4.2. Future Work

The work presented in this research thesis provides a solid starting point in the examination of the nanoscale physical effects of e-beam irradiation on food. Because some carbon-based nanomaterials have been found to be toxic to mammals, the nanostructures found in this work generate questions regarding the safety of e-beam irradiated foods, questions that can be answered through cytotoxicity studies. Previous studies on the safety of irradiated foods focused on overall health of the test subject, measuring growth rate, reproductive ability of the test subject, and hematology and histopathology measurements.[2-5] Cytotoxicity studies would provide for measuring health of the test subject on a smaller scale. Finally, developing an

understanding of the mechanism of nanostructure formation can help us to design modifications to the current irradiation process so that the formation of nanostructures does not occur.

4.3. Final Remarks

This work does not intend to put e-beam irradiation in a negative light, only address an issue not previously noted. Should irradiation methods prevail, we suggest that changes be made to the irradiation process, such as establishing allowed dosages, so that nanostructures do not form, rather than abandon sterilization by ionizing irradiation. Also, results form cytotoxicity studies of the nanostructures found from the work in this thesis may also warrant additions to the metric points in testing the safety of irradiated foods and food packaging.

4.4. References

(1) Peter, K.V., *Handbook of herbs and spices, Vol. 3*. CRC Press: Boca Raton, FL, **2006**.

(2) Read, M.S.; Trabosh, H.M.; Worth, W.S.; Kraybill, H.F.; Witt, N.F. Short-Term Rat-Feeding Studies with Gamma-Irradiated Food Products. *Toxicol. Appl. Pharm.* **1959**, *1*, 417-425.

(3) Bubl, E.C.; Butts, J.S. The Growth, Breeding and Longevity of Rats Fed Irradiated or Non-Irradiated Pork. *J. Nutr.* **1960**, *70*, 211-218.

(4) Burns, C.H.; Abrams, G.D.; Brownell, L.E. Growth, Reproduction, Mortality, and Pathologic Changes in Rats Fed Gamma-Irradiated Potatoes. *Toxicol. Appl. Pharm.* **1960**, *2*, 111-131.

(5) Tinsley, I.J.; Bone, J.F.; Bubl, E.C. The Growth, Reproduction, Longevity, and Histopathology of Rats Fed Gamma-Irradiated Peaches. *Toxicol. Appl. Pharm.* **1963**, *5*, 464-477.